NATIONAL ADVISORY COMMITTEE FOR AERONAUTICS

TECHNICAL NOTE 3212

A NONLINEAR THEORY OF BENDING AND BUCKLING OF THIN ELASTIC SHALLOW SPHERICAL SHELLS

By A. Kaplan and Y. C. Fung

California Institute of Technology

Washington
August 1954

NATIONAL ADVISORY COMMITTEE FOR AERONAUTIC

TECHNICAL NOTE 3212

A NONLINEAR THEORY OF BENDING AND BUCKLING OF THIN ELASTIC SHALLOW SPHERICAL SHELLS

By A. Kaplan and Y. C. Fung

SUMMARY

A shallow spherical dome subjected to lateral pressure is a structure for which the deformation departs appreciably from the linear theory at relatively small values of the deflection amplitude. It is also one for which the buckling process is characterized by a rapid decrease in the equilibrium load once the buckling load has been surpassed. For structures having this type of buckling characteristics the question arises as to whether the proper buckling criterion to apply is the classical criterion, which considers equilibrium with respect to infinitesimal displacements, or the finite-displacement "energy criterion" proposed by Tsien.

In this paper the problem of the finite displacement and buckling of a shallow spherical dome is investigated both theoretically and experimentally. In the theoretical approach the nonlinear equations are converted into a sequence of linear equations by expanding all of the variables in powers of the center deflection and then equating the coefficients of equal powers. The basic parameter for the shallow dome λ is proportional to the ratio of the central height of the dome h to its thickness t. For small values of this ratio the expansions converge rapidly and enough terms are computed to determine the buckling load according to the classical criterion. For higher values of h/t, convergence deteriorates rapidly and it was not possible to determine the buckling load with the number of terms which were computed. However even for these higher values of h/t the deflection shapes are determined for deflection amplitudes below the amplitude at which buckling occurs. These deflection shapes are characterized by their rapid change as h/t increases and by the fact that, over most of the range of h/t studied, the maximum deflection does not occur at the center of the dome.

Experimental results seem to indicate that the classical criterion of buckling is applicable to very shallow spherical domes for which the theoretical calculation was made. A transition to energy criterion for higher domes is also indicated.

INTRODUCTION

The development of the theory of bending of thin-walled spherical shells has a long record. A survey of the problem can be found in references 1 and 2. The fundamental equations are developed by Hans Reissner[1] (1912) who shows that, for a thin-walled spherical dome that is not shallow, the membrane stresses in the shell maintain equilibrium with the external pressure, while the bending of the shell has relatively little effect except near the edge of the shell where the shell adjusts itself quickly to the prescribed boundary conditions. Bending in the shell is therefore essentially an "edge effect" or "boundary layer" phenomenon. Asymptotic solutions of the bending problem have been obtained by Blumenthal (1912), Havers (1935), Jacobsen (1937), and others[1] on the basis that the parameter $(R/t)^2$ is very large, where R is the radius of the spherical shell and t, its wall thickness. Both symmetrical and nonsymmetrical loading and edge conditions have been treated, including the case of a dome supported on columns.

The asymptotic solutions are, however, not valid for shallow spherical shells,[2] for which the effect of edge conditions is no longer limited to a thin layer near the edge and the interaction of bending and membrane stresses is strong. In 1946 Eric Reissner (ref. 3) developed the governing equations for shallow spherical shells on the explicit assumption that the ratio h/a is so small that $(h/a)^2$ is negligible in comparison with h/a, h being the height of the dome and a its radius (see fig. 1). A few special cases are solved in reference 3.

Reissner's solutions are based on linearized equations. Since the effect of bending on the membrane stresses is strong in the case of a shallow dome, one naturally asks the question: To what extent is the process of linearization valid? Expressed in terms of the ratio of the vertical deflection at the center of the dome to the wall thickness w_o/t, the question is: How soon does the solution deviate from linearity as w_o/t increases?

To answer this question the nonlinear problem is treated in the present paper. The particular problem of a shallow spherical shell with a clamped edge carrying a uniform pressure is chosen so that a convenient experimental comparison can be made. It is shown that the nonlinear character depends upon a parameter λ which is defined as

$$\lambda^2 = \sqrt{12\left(1 - \mu^2\right)}\frac{a^2}{tR} \tag{1}$$

---

[1]See Timoshenko's book, reference 1, for references to original papers.

[2]By shallow is meant a spherical segment for which the ratio of the height to the base radius is small, say, less than 1/8.

where μ is the Poisson's ratio and t, a, and R are as previously defined (see fig. 1). The range of w_o/t in which the linear solution is valid is small indeed. For example, at $\lambda = 4$, the equilibrium pressure given by the linear solution is, respectively, 9, 23, and 50 percent too high when w_o/t is 0.1, 0.25, and 0.5.

Consider now the problem of buckling of thin-walled spherical shells. For a complete sphere under uniform pressure, the classical solution, on the basis of linearized equations, is obtained by Zoelly (1915), Schwerin (1922), and Van der Neut (1932). (See ref. 2, p. 491.) The buckling stress σ_{cr} is given by

$$\sigma_{cr} = \frac{Et}{R\sqrt{3\left(1 - \mu^2\right)}} \qquad \left(\sigma_{cr} = \frac{R}{2t}\, q_{cr}\right) \qquad (2)$$

where q_{cr} is the critical value of external pressure. This stress has the same magnitude as the critical stress for an axially compressed cylindrical shell of radius R and of thickness t. It is relatively high in comparison with experimental results. The corresponding buckling mode predicted by the theory is also at variance with laboratory experience. To reconcile the differences between theory and experiment Von Kármán and Tsien in 1939 (ref. 4) introduced a new concept into the theory of elasticity: the "lower buckling load." They discovered that for values of pressure q considerably below that given by equation (2) quite different stable states of equilibrium exist, which could be revealed only by abandoning the classical linearization of the problem. The minimum of such values of q is the lower buckling load q_K. If q exceeds q_K, the chances are great that buckling will occur. In reference 4 the lower buckling load is computed (subject to a number of simplifying assumptions) with respect to a special class of buckling modes. Friedrichs in reference 5 avoids some of the arbitrary assumptions by applying asymptotic integration in the manner of a boundary-layer theory. Application of Friedrichs' equations, however, yields no minimum buckling load, and it is pointed out (ref. 6) that the minimum obtained in reference 4 is due to the special form of displacements assumed in that investigation.

The final "energy criterion" of buckling is formulated by Tsien in reference 6. It is stated that under average laboratory and actual service conditions the most probable equilibrium state is the state with the lowest possible energy level. In other words it is assumed that there are disturbances of sufficient magnitude so that the transitions from higher energy levels to lower energy levels are always possible. Two conditions must be satisfied in defining the "possible energy levels": (1) the corresponding external forces and internal stresses must be in

equilibrium; (2) the geometric restraint and loading conditions, if any, must be satisfied. Tsien points out that these necessary conditions for possible energy levels are not checked in references 4 and 5. When the check is applied (ref. 6), a lower buckling load is obtained for spherical shells on the basis of Friedrichs' equations. The agreement with experiments is good.

It appears that these arguments apply equally well to spherical domes and to the complete sphere. Therefore, the first theoretical question to be settled is whether the "classical criterion" of buckling or the "energy criterion" should be used in calculating the critical buckling load. The classical buckling criterion is based on the assumption that a given state of equilibrium of a shell becomes unstable when there are equilibrium positions infinitesimally near to that state of equilibrium under the same external load. Thus in applying the classical criterion an equilibrium state is compared with its neighboring equilibrium states and the incipient buckling is revealed by a negative slope of the load-deflection curve, that is, when an increase of deflection corresponds to a decrease in the corresponding applied load. The important contrast between the classical criterion and the energy criterion is that in the former only a continuous load-deflection process is considered, while in the latter a jump to the state of lower energy level is permitted even though the intervening states involve higher energy levels. The linearization of the governing equations, ordinarily made purely for mathematical simplicity, should not be regarded as a part of the classical criterion.

Although the energy criterion seems plausible, nevertheless it can be verified only by comparison with experiments. The energy criterion necessarily yields a buckling load which is never greater than that given by the classical criterion. If there is a wide difference between the two buckling loads the problem becomes simply to choose the criterion that gives closer agreement with the experiments.

For shallow spherical domes the buckling load calculated on the basis of the classical criterion, but <u>without</u> linearizing the governing equations, is known only in very few cases. In the comparison with experiments presented in figure 20 of reference 6, the curve labeled "classical theory" is really the one given by equation (2), which is applicable to a complete sphere and is calculated from linearized equations. When the nonlinear equations applicable to a shallow spherical dome are used the buckling load is lower than that given by equation (2). For example, when $\lambda = 4$ the calculation of the present report gives a buckling load which is about one-half that given by equation (2). Thus the wide difference between the classical theory and experiments exhibited in the figure cited above may be entirely caused by an improper mathematical process.

To clarify the argument further, consider the case of a flat arch, as a two-dimensional analog of the spherical dome. For such an arch two buckling modes are possible. If the arch rise is high, it buckles in the mode shown in figure 2: the center line of the arch remains essentially "inextensional." If the arch rise is small, it may buckle downward with a sudden reversal of curvature, as shown in figure 3: a phenomenon sometimes described as "oil-canning" or "durchschlag." The axial compressive strain plays a dominant role in the latter case and linearization of the governing equations is not permissible. A detailed study made in reference 7 shows that in practice the classical criterion agrees better with experiments, except for very low arches (arches whose rise is of the order of the wall thickness) for which the energy hump tends to vanish and the gap between the two criteria tends to be closed.

For shallow spherical domes the prevailing buckling mode is of the oil-canning type, in which the membrane stress plays an important part, and is basically a nonlinear phenomenon.

There exists only one paper on the oil-canning of shallow spherical domes based on the classical criterion. This is Biezeno's work (ref. 8) which treats a shallow dome whose edge is free to expand so that the membrane stress in the radial direction vanishes on the edge; and the dome is subjected to a concentrated load acting at the center. The following equations (which are equivalent to those of the present paper) are obtained:

$$r^2 \frac{d^2 v_o}{dr^2} + r \frac{dv_o}{dr} - v_o + r^2\left(\frac{r}{R} + \psi\right) + (2 - \mu) \frac{r^2}{R} \psi +$$

$$\frac{1 - \mu}{2} r\psi^2 = - \frac{Pr}{2\pi} \frac{(1 - \mu^2)}{Et}\left(\frac{1}{R} + \frac{d\psi}{dr}\right) \tag{3}$$

$$r^2 \frac{d^2\psi}{dr^2} + r \frac{d\psi}{dr} - \psi = \frac{r}{D}\left[\frac{P}{2\pi} + rN_r\left(\frac{r}{R} + \psi\right)\right] \tag{4}$$

$$N_r = \frac{Et}{1 - \mu^2}\left[\frac{dv_o}{dr} + \mu \frac{v_o}{r} + \left(\frac{r}{R} + \frac{1}{2} \psi\right)\psi\right] \tag{5}$$

where P is the central load, $\psi = \frac{dw}{dr}$ is the slope of the deflection surface in a meridional section, w being the radial displacement normal

to the original spherical shell, and v_o is the component of displacement normal to the axis of symmetry, that is (see fig. 1),

$$v_o = u \cos \theta - w \sin \theta \tag{6}$$

Other symbols are defined in the list which follows this section. Biezeno makes the following simplifying assumptions to obtain a solution: (1) that the term on the right-hand side of equation (3) may be neglected; (2) that in equations (3), (5), and on the right-hand side of equation (4) the slope of the radial displacements ψ can be written as

$$\psi = \psi_1 = C_1 \frac{r}{R} + C_2 \frac{r}{R} \log \frac{a}{r} \tag{7}$$

where C_1 and C_2 are two undetermined constants. Equation (4) is then solved with proper boundary conditions. Let the solution be denoted by ψ_2, which, of course, is different in form from equation (7). Biezeno then determines the constants C_1 and C_2 by requiring that ψ_1 and ψ_2 yield the same values of vertical displacement at the edge of the plate ($r = a$) and at the center ($r = 0$). The load-deflection curve can then be calculated from equation (7) and the buckling load determined.

The influence of Biezeno's simplifying assumptions on the buckling load is not easy to assess; and there exist no experimental results to compare with the theory.

The case considered in the present paper is that of a shell clamped at the edge and subjected to uniform lateral pressure. The equations of equilibrium (equivalent to eqs. (3), (4), and (5)) are solved as perturbation series expressed in powers of the parameter w_o/t, that is, the ratio of the deflection on the axis of symmetry and the wall thickness of the shell. The load-deflection curve so determined is used to obtain the buckling load.

Relatively few assumptions are made in the present calculation. Unfortunately the perturbation series seems to deteriorate rapidly for large values of λ, so the result is satisfactory only for λ of order 5 or smaller. In this range of λ the buckling loads computed on the basis of the classical criterion agree quite well with experiments.

On the other hand the calculation of the buckling load on the basis of Tsien's energy criterion also offers considerable difficulty. If the formulas of reference 6 are extended to cover the shallow shells studied in the present paper it is found that the so-called "lower buckling load"

has an equal or higher value than that given in equation (2) when $\lambda \leq 10$. This unreasonable result is obtained because the energy expressions and the mode shape assumed are not sufficiently accurate. It is not clear how to improve the results. Theoretical deflection curves derived from the bending theory do not permit a very simple representation. In any case, the refinement of Tsien's calculation would have been a major endeavor. For the same reason the calculation of the buckling load on the basis of classical criterion using the Rayleigh-Ritz method is not pursued. Therefore the most convenient theoretical determination of the critical buckling load remains an open question.

In order to do justice to either the classical criterion or the energy criterion, further theoretical study must be made for λ in the range, say, from 5 to 15. A study of all available experimental data on the subject seems to show that the classical criterion of buckling holds for very shallow spherical domes, while a transition to energy criterion takes place at some intermediate values of λ of order 6.

One more point should be mentioned before the presentation of the main analysis. In reference 5, Friedrichs suggests that it may be possible that a boundary layer occurs at the edge of a certain segment, the width of which in its turn shrinks to zero with the thickness of the shell. This suggestion seems plausible because as the shell becomes thinner and thinner the bending of the shell becomes less and less important. In the limit $t \to 0$ the deflected surface must be an "applicable" surface of the original.[3] In the upper part of figure 4 the shell represented by the dotted line is applicable to that represented by the solid line; in other words, a deformation of the solid line into the dotted line involves no strain energy due to the membrane stresses. To account for the small but finite bending energy of the shell the deflection surface may take the form represented by the lower part of figure 4. A boundary layer may be developed at the segment angle α. This conjecture, however, turns out to be improbable for a shell subjected to uniform external pressure; since it can be shown that the segment angle α tends to zero at a higher order in t (the shell thickness) than does the boundary-layer thickness. Therefore the boundary layer can be developed only at a pole $\alpha = 0$ which is the case presented in reference 5.

The investigation presented in the present paper was conducted at the California Institute of Technology under the sponsorship and with the financial assistance of the National Advisory Committee for Aeronautics.

---

[3]Two surfaces are called "applicable" to each other in differential geometry if one can deform into the other by continuous bending without stretching or tearing the surface.

SYMBOLS

A_n, B_n, C_n, D_n, E_n	integration constants
a	base radius of shell
a_n, b_n, c_n	coefficients in power-series expansion of F_2 in terms of λx; see equation (A5)
$D = \frac{Et^3}{12(1 - \mu^2)}$	
d_n, g_n, h_n	coefficients in power-series expansion of F_2 in terms of λx; see equation (A7)
E	Young's modulus
F_n	functions of f_n and w_n; see equation (28)
f_n	coefficient of expansion for S_r in powers of W_o
h	central height of shell above base plane
K	constant; see equation (41)
$k = \sqrt{12(1 - \mu^2)}$	
M_r	radial bending moment per unit length
M_t	circumferential bending moment per unit length
N_r	radial membrane force per unit length
N_t	circumferential membrane force per unit length
$P = \frac{1 - \mu^2}{E}\left(\frac{a}{t}\right)^4 q$	
p_n	coefficient of expansion for P in powers of W_o
Q	shear force per unit length perpendicular to middle surface of shell
q	pressure on surface of shell; positive when directed downward

R	initial radius of curvature of shell
r	horizontal distance from axis of symmetry of shell
$S_r = \frac{a^2}{Et^3} N_r$	
$S_t = \frac{a^2}{Et^3} N_t$	
t	thickness of shell
u	radial displacement of middle surface of shell measured tangential to initial surface and positive in outward direction
$W = w/t$	
$W_o = w_o/t$	
w	vertical displacement of middle surface of shell measured perpendicular to initial surface and positive in downward direction
w_n	coefficient of expansion for W in powers of W_o
$w_o = w(r = 0)$	
$x = r/a$	
z_o	initial distance of point on middle surface of shell above base plane
α	segment angle of a possible deflected surface
$\alpha_n, \beta_n, \gamma_n$	functions of θ_n and φ_n; see equations (35)
β	semi-included angle of shell
δ	finite-difference interval
ϵ_r	radial strain
ϵ_t	circumferential strain

$\eta = x^2/4$

$\theta = \sin^{-1}(r/R)$

θ_n particular integral of equations (26) for f_n

$\lambda^2 = \frac{ka^2}{Rt} \approx 4\sqrt{3(1 - \mu^2)}\,\frac{h}{t}$

μ Poisson's ratio

$\rho = \text{bei}\,\lambda\,\text{ber}'\lambda + (1 - \text{ber}\,\lambda)\,\text{ber}'\lambda$

φ circumferential position angle

φ_n integrals of w_n; see equations (29)

Subscript:

cr critical

THEORETICAL ANALYSIS

Derivation of Equations

Consider the spherical shell segment of radius R, base diameter 2a, height h, and constant thickness t shown in figure 1. The initial position of a point in the central surface is given by the cylindrical coordinates r, φ, and z_o, where r is the radial distance from the center, measured parallel to the base, φ is the circumferential angle, and z_o is the vertical distance, measured upward, from the base plane. It is assumed that h/a is small enough that

$$\left.\begin{aligned} z_o &= h + \sqrt{R^2 - r^2} - R \approx h - \frac{1}{2}\frac{r^2}{R} \\ \frac{dz_o}{dr} &\approx -\frac{r}{R} \end{aligned}\right\} \tag{8}$$

The deformation of the middle surface is assumed to be radially symmetric and is therefore specified by u, measured tangential to the middle surface in the outward radial direction, and w, measured perpendicular to the middle surface in the downward direction. The deflections

are considered to be finite, but small enough so that $\left(\frac{dw}{dr}\right)^2$ can be neglected with respect to unity.

Since, under these conditions, the magnitudes of vectors tangential to the middle plane are equal to their components parallel to the base plane, the equations for forces and moments in the middle plane are identical with those for a flat plate. That is,

$$\frac{d}{dr}\left(rM_r\right) - M_t - rQ = 0 \tag{9}$$

$$\frac{d}{dr}\left(rN_r\right) - N_t = 0 \tag{10}$$

where N_r and N_t are, respectively, the radial and circumferential membrane stresses, M_r and M_t are the corresponding bending moments, and Q is the shear stress in the direction perpendicular to the deformed middle surface. Vertical equilibrium of a central cylindrical section of radius r (fig. 5) requires that

$$Q = -\frac{1}{r}\int_0^r rq\,dr + N_r\left(\frac{dz_o}{dr} - \frac{dw}{dr}\right) \tag{11}$$

where q is the applied pressure. Substituting equation (11) into equation (9) and using the approximation equations (8) result in

$$\frac{d}{dr}\left(rM_r\right) - M_t + \int_0^r rq\,dr + rN_r\left(\frac{r}{R} + \frac{dw}{dr}\right) = 0 \tag{12}$$

The bending moments are expressed in terms of the deflections using the strain-deflection relations

$$\left.\begin{aligned} \epsilon_r &= \frac{du}{dr} + \frac{1}{2}\left(\frac{dw}{dr}\right)^2 - \frac{w}{R} \\ \epsilon_t &= \frac{u}{r} - \frac{w}{R} \end{aligned}\right\} \tag{13}$$

where ϵ_r and ϵ_t are the longitudinal strains of the middle surface in the radial and circumferential directions, respectively. Then

$$\left.\begin{aligned} N_r &= \frac{Et}{1-\mu^2}\left[\frac{du}{dr} - \frac{w}{R} + \frac{1}{2}\left(\frac{dw}{dr}\right)^2 + \mu\left(\frac{u}{r} - \frac{w}{R}\right)\right] \\ N_t &= \frac{Et}{1-\mu^2}\left\{\frac{u}{r} - \frac{w}{R} + \mu\left[\frac{du}{dr} - \frac{w}{R} + \frac{1}{2}\left(\frac{dw}{dr}\right)^2\right]\right\} \\ M_r &= -D\left(\frac{d^2w}{dr^2} + \frac{\mu}{r}\frac{dw}{dr}\right) \\ M_t &= -D\left(\frac{1}{r}\frac{dw}{dr} + \mu\frac{d^2w}{dr^2}\right) \end{aligned}\right\} \tag{14}$$

where $D = \dfrac{Et^3}{12\left(1-\mu^2\right)}$.

Using these expressions for M_r and M_t, equation (12) becomes

$$Dr\frac{d}{dr}\left[\frac{1}{r}\frac{d}{dr}\left(r\frac{dw}{dr}\right)\right] = rN_r\left(\frac{r}{R} + \frac{dw}{dr}\right) + \int_0^r qr\,dr \tag{15}$$

This is the first basic equation. Now from equations (13)

$$\frac{u}{r} = \epsilon_t + \frac{w}{R} = \frac{1}{Et}\left(N_t - \mu N_r\right) + \frac{w}{R}$$

so that

$$\frac{du}{dr} = \frac{1}{Et}\frac{d}{dr}\left(rN_t - \mu rN_r + Et\frac{wr}{R}\right) \tag{16}$$

These values are substituted in the first of equations (14) to obtain a second relation between N_t and N_r:

$$N_r = \frac{Et}{1 - \mu^2}\left[\frac{1}{Et}\frac{d}{dr}\left(rN_t - \mu rN_r + Et\,\frac{wr}{R}\right) - \frac{w}{R} + \frac{1}{2}\left(\frac{dw}{dr}\right)^2 + \frac{\mu}{Et}\left(N_t - \mu N_r\right)\right] \tag{17}$$

Combining this equation with equation (10), the second basic equation is obtained:

$$r\,\frac{d}{dr}\,\frac{1}{r}\,\frac{d}{dr}\left(r^2N_r\right) + \frac{1}{2}\,Et\left(\frac{dw}{dr}\right)^2 + Et\,\frac{r}{R}\,\frac{dw}{dr} = 0 \tag{18}$$

Knowing w and N_r, N_t can be obtained from equation (10). In the problem to be studied q is a constant so that equation (15) becomes

$$D\,\frac{d}{dr}\left[\frac{1}{r}\,\frac{d}{dr}\left(r\,\frac{dw}{dr}\right)\right] = N_r\left(\frac{r}{R} + \frac{dw}{dr}\right) + \frac{1}{2}\,qr \tag{19}$$

These equations are transformed into nondimensional form by the use of the following variables:

$$\left.\begin{aligned} x &= \frac{r}{a} \\ W &= \frac{w}{t} \\ k^2 &= 12\left(1 - \mu^2\right) \\ S_r &= \frac{a^2}{Et^3}\,N_r \\ S_t &= \frac{a^2}{Et^3}\,N_t \\ P &= \frac{1 - \mu^2}{E}\left(\frac{a}{t}\right)^4 q \\ \lambda^2 &= \frac{ka^2}{Rt} \end{aligned}\right\} \tag{20}$$

The parameter λ^2 can also be expressed as (see fig. 1)

$$\left.\begin{aligned} \lambda^2 &= k\frac{R}{t}\sin^2\beta \approx k\frac{R\beta^2}{t} \\ \text{or} \\ \lambda^2 &= k\frac{h}{t}\frac{\sin^2\beta}{1-\cos\beta} = k\frac{h}{a}(1+\cos\beta) \approx 2k\frac{h}{t} \end{aligned}\right\} \tag{21}$$

Thus for the assumed range of β, λ^2 is proportional to the ratio of the central height of the dome to its thickness and can therefore be interpreted as representing the ratio of the compression stiffness to the bending stiffness.

Upon substituting these new variables, equations (18), (19), and (10) become

$$\frac{d}{dx}\left[\frac{1}{x}\frac{d}{dx}\left(x^2S_r\right)\right] + \frac{1}{2x}\left(\frac{dW}{dx}\right)^2 + \frac{\lambda^2}{k}\frac{dW}{dx} = 0 \tag{22}$$

$$\frac{1}{x}\frac{d}{dx}\left[\frac{1}{x}\frac{d}{dx}\left(x\frac{dW}{dx}\right)\right] - k\left(\lambda^2 + \frac{k}{x}\frac{dW}{dx}\right)S_r = 6P \tag{23}$$

$$S_t = \frac{d}{dx}\left(xS_r\right) \tag{24}$$

With $\lambda = 0$ ($R = \infty$) these are Kármán's equations for the finite deflection of a flat plate, expressed in polar coordinates. Their derivation is exactly analogous to Chien's derivation of the equations for the finite deflection of a flat circular plate (ref. 9).

Expansion in Terms of $W_o(=w_o/t)$

As in Chien's paper (ref. 9) the procedure used for solving equations (22), (23), and (24) is to consider the center deflection ratio $W(0) = W_o$ as a parameter and to expand all of the variables in powers of W_o. Thus

$$\left.\begin{aligned} P &= p_1 W_o + p_2 W_o^2 + p_3 W_o^3 + \cdots \\ W &= w_1(x) W_o + w_2(x) W_o^2 + w_3(x) W_o^3 + \cdots \\ S_r &= f_1(x) W_o + f_2(x) W_o^2 + f_3(x) W_o^3 + \cdots \end{aligned}\right\} \tag{25}$$

These expansions are valid for small enough values of the deflection ratio W_o, but their exact range of convergence is unknown. For the case of the flat circular plate Chien obtained good convergence for values of W_o as high as 4.

Substitution of these series in equations (22) and (23) and the equating of equal powers of W_o result in a sequence of pairs of simultaneous equations for f_n and w_n. Each of these pairs of equations can then be combined to obtain an equation for f_n alone

$$\frac{1}{x^3}\frac{d}{dx}\left\{\frac{1}{x}\frac{d}{dx}\left[x^5\frac{d}{dx}\left(\frac{1}{x}\frac{df_n}{dx}\right)\right]\right\} + \lambda^4 f_n = -\frac{6}{k}\lambda^2 p_n - F_n \tag{26a}$$

or

$$\frac{d^4 f_n}{dx^4} + \frac{6}{x}\frac{d^3 f_n}{dx^3} + \frac{3}{x^2}\frac{d^2 f_n}{dx^2} - \frac{3}{x^3}\frac{df_n}{dx} + \lambda^4 f_n = -\frac{6}{k} p_n \lambda^2 - F_n \tag{26b}$$

plus an equation for w_n in terms of f_n

$$w_n = \frac{k}{\lambda^2 x}\frac{d}{dx}\left(x^2 f_n\right) - \frac{k^3}{\lambda^2}\varphi_n + E_n \tag{27}$$

where E_n is a constant and F_n and φ_n are the following functions:

$$
\left.
\begin{aligned}
F_1 &= 0 \\
F_2 &= k\lambda^2 \frac{1}{x} f_1 \frac{dw_1}{dx} + \frac{1}{x} \frac{d}{dx}\left[\frac{1}{x} \frac{d}{dx} \frac{1}{2}\left(\frac{dw_1}{dx}\right)^2\right] \\
F_3 &= k\lambda^2 \frac{1}{x}\left(f_2 \frac{dw_1}{dx} + f_1 \frac{dw_2}{dx}\right) + \frac{1}{x} \frac{d}{dx}\left[\frac{1}{x} \frac{d}{dx}\left(\frac{dw_1}{dx} \frac{dw_2}{dx}\right)\right] \\
F_4 &= k\lambda^2 \frac{1}{x}\left(f_1 \frac{dw_3}{dx} + f_2 \frac{dw_2}{dx} + f_3 \frac{dw_1}{dx}\right) + \\
&\quad \frac{1}{x} \frac{d}{dx}\left\{\frac{1}{x} \frac{d}{dx}\left[\frac{dw_1}{dx} \frac{dw_3}{dx} + \frac{1}{2}\left(\frac{dw_2}{dx}\right)^2\right]\right\}
\end{aligned}
\right\} \tag{28}
$$

$$
\left.
\begin{aligned}
\varphi_1 &= 0 \\
\varphi_2 &= \int_0^x \frac{1}{2}\left(\frac{dw_1}{dx}\right)^2 \frac{dx}{x} \\
\varphi_3 &= \int_0^x \frac{dw_1}{dx} \frac{dw_2}{dx} \frac{dx}{x} \\
\varphi_4 &= \int_0^x \left[\frac{1}{2}\left(\frac{dw_2}{dx}\right)^2 + \frac{dw_1}{dx} \frac{dw_3}{dx}\right] \frac{dx}{x}
\end{aligned}
\right\} \tag{29}
$$

Upon making the substitution $4\eta = x^2$ equation (26a) becomes

$$\frac{d^2}{d\eta^2}\left(\eta^3 \frac{d^2}{d\eta^2} f_n\right) + \lambda^2 \eta f_n = -\frac{3}{8k} \lambda^2 p_n - \frac{1}{16} F_n \tag{30}$$

which can be recognized as the equation for the lateral deflection of a linearly tapered beam on an elastic support whose spring constant is a linear function of position along the span. This interpretation is useful in the numerical work which follows.

The solution of the homogeneous part of equation (26a) or (26b), that is, the complementary function, is

$$f_n = \frac{1}{x}\left(A_n \operatorname{ber}'\lambda x + B_n \operatorname{bei}'\lambda x + C_n \operatorname{ker}'\lambda x + D_n \operatorname{kei}'\lambda x\right)$$

where

$$\operatorname{ber}' z = \frac{d}{dz} \operatorname{ber} z$$

and the ber and bei functions are defined in terms of J_o, the zero-order Bessel function of the first kind, by

$$J_o\left(zi^{3/2}\right) = \operatorname{ber} z + i \operatorname{bei} z$$

with an analogous relation between ker z, kei z, and $K_o\left(zi^{3/2}\right)$

Boundary Conditions

The boundary conditions for a clamped-edge shell subjected to a radially symmetric distributed load are

$$\left.\begin{array}{ll} \text{at } x = 0, & \\ & \dfrac{dw}{dx} = 0, \quad S_r \text{ is finite} \\ \text{at } x = 1, & \\ & w = \dfrac{dw}{dx} = u = 0 \end{array}\right\} \tag{31}$$

To satisfy the first two conditions it is necessary that

$$C_n = D_n = 0$$

In terms of the expansion coefficients, equations (25), the remaining boundary conditions become

$$\left.\begin{aligned} w_n &= 0 \\ \frac{dw_n}{dx} &= 0 \\ (1 - \mu)f_n + x\frac{df_n}{dx} &= 0 \end{aligned}\right\} \quad x = 1 \tag{32a}$$

Because of the nature of the expansion there is the additional condition that

$$w_n(0) = \begin{cases} 1, & n = 1 \\ 0, & n \geq 2 \end{cases} \tag{32b}$$

The constant E_n in equation (27) can be eliminated by combining equations (32a) and (32b) so that the boundary condition on w_n becomes

$$w_n(0) - w_n(1) = \begin{cases} 1, & n = 1 \\ 0, & n \geq 2 \end{cases} \tag{32c}$$

Let θ_n be the particular solution corresponding to F_n, on the right-hand side of equation (26a); then the complete solution for f_n becomes

$$f_n = \frac{1}{x}\left(A_n \operatorname{ber}'\lambda x + B_n \operatorname{bei}'\lambda x\right) + \theta_n - \frac{6}{k}\frac{p_n}{\lambda^2} \tag{33}$$

while

$$w_n = \frac{k}{\lambda}\left(A_n \operatorname{bei}\lambda x - B_n \operatorname{ber}\lambda x\right) - \frac{k}{\lambda^2 x}\frac{d}{dx}\left(x^2\theta_n\right) - \frac{k}{\lambda^2}\varphi_n + E_n$$

Substitution of these values into boundary conditions (32) and their solution for A_n, B_n, and p_n result in

$$A_n = \frac{1}{\rho}\left[\alpha_n \operatorname{ber}'\lambda + \beta_n(1 - \operatorname{ber}\lambda)\right] \tag{34a}$$

$$B_n = \frac{1}{\rho}\left(\alpha_n \operatorname{bei}'\lambda - \beta_n \operatorname{bei}\lambda\right) \tag{34b}$$

$$p_n = -\frac{k\lambda^2}{6(1-\mu)\rho}\Bigg(\Big\{(1+\mu)\left[(\operatorname{ber}'\lambda)^2 + (\operatorname{bei}'\lambda)^2\right] + \lambda(\operatorname{ber}'\lambda \operatorname{bei}\lambda - \operatorname{bei}'\lambda \operatorname{ber}\lambda)\,\alpha_n\Big\} + \Big\{(1+\mu)\left[(1-\operatorname{ber}\lambda)\operatorname{ber}'\lambda - \operatorname{bei}\lambda \operatorname{bei}'\lambda\right] + \lambda \operatorname{bei}\lambda\Big\}\beta_n\Bigg) + \gamma_n \tag{34c}$$

where

$$\rho = \operatorname{bei}\lambda \operatorname{ber}'\lambda + (1 - \operatorname{ber}\lambda)\operatorname{ber}'\lambda \tag{35a}$$

$$\alpha_n = \frac{1}{\lambda}\left|\frac{1}{x}\frac{d}{dx}\left(x^2\theta_n\right)\right|_{x=0}^{x=1} + \frac{k^2}{2\lambda}\varphi_n(1) \tag{35b}$$

$$\beta_n = \frac{1}{\lambda^2}\left\{\frac{d}{dx}\left[\frac{1}{x}\frac{d}{dx}\left(x^2\theta_n\right)\right]\right\}_{x=1} \tag{35c}$$

$$\gamma_n = \frac{k\lambda^2}{6}\left(\theta_n + \frac{1}{1-\mu}\frac{d\theta_n}{dx}\right)_{x=1} \tag{35d}$$

First-Order Solution

The particular solution θ_1 of the first-order equation is zero and the equations for A_1, B_1, and p_1 reduce to

$$A_1 = \frac{\lambda \operatorname{ber}'\lambda}{k\rho}$$

$$B_1 = \frac{\lambda \operatorname{bei}'\lambda}{k\rho}$$

$$p_1 = \frac{\lambda^2}{6(1-\mu)\rho}\left\{(1+\mu)\left[(\operatorname{ber}'\lambda)^2 + (\operatorname{bei}'\lambda)^2\right] + \lambda(\operatorname{ber}'\lambda \operatorname{bei}\lambda - \operatorname{bei}'\lambda \operatorname{ber}\lambda)\right\} \tag{36}$$

The values of A_1, B_1, and p_1 are given in table 1, while the values of w_1 and f_1 are given in tables 2 and 3 and are plotted in figures 6 and 7, respectively. This first-order solution is identical with the linear solution previously found by Reissner (ref. 3).

For the higher order equations no solution was found in terms of known functions and so it was necessary to resort to power-series expansion and numerical methods.

Power-Series Solutions

Judging from the work of Chien (ref. 9) it was felt that calculation of the first two terms, p_1 and p_2, of the expansion for the pressure P would permit at least an approximate determination of the buckling load. Therefore a power-series solution for θ_2 was obtained even though it was realized that the succeeding solutions could not be obtained by this method because of the involved form of the functions F_n. The procedure and formulas used are shown in appendix A. Since the expansions are all in terms of λx it was necessary to restrict the calculations to values of $\lambda \leqq 8$. The values of p_2 obtained are shown in table 4 and plotted in figure 8. These values are negative for small values of λ, but become positive at $\lambda = 6.5$ and are rapidly increasing at $\lambda = 8$. Since buckling can occur only when some of the p_n's are negative it was clearly necessary to obtain the higher order terms of p_n. These additional values of p_n were obtained numerically.

Numerical Solutions

The differential equations (26) contain the unknown parameter p_n and also have the unwieldy boundary condition that S_r is finite at $x = 0$. As a result a complete numerical solution would be very difficult.

Therefore only the particular solution is determined numerically, using arbitrary boundary conditions. The required boundary conditions are then satisfied using the known solution of the homogeneous equation.

In terms of the finite-difference approximations

$$\left.\begin{aligned}
f'(x) &= \frac{1}{2\delta}\left[f(x+\delta) - f(x-\delta)\right] \\
f''(x) &= \frac{1}{\delta^2}\left[f(x+\delta) - 2f(x) + f(x-\delta)\right] \\
f'''(x) &= \frac{1}{2\delta^3}\left[f(x+2\delta) - 2f(x+\delta) + 2f(x-\delta) - f(x-2\delta)\right] \\
f^{iv}(x) &= \frac{1}{\delta^4}\left[f(x+2\delta) - 4f(x+\delta) + 6f(x) - 4f(x-\delta) + f(x-2\delta)\right]
\end{aligned}\right\} \quad (37)$$

where δ is the difference interval; equation (26a) (with the constant term $-\frac{3}{8}\frac{p_n\lambda^2}{k}$ omitted) becomes

$$\left(\frac{6}{\delta^4} - \frac{6}{\delta^2 x^2} + \lambda^4\right)\theta_n(x) - \left(\frac{4}{\delta^4} + \frac{6}{\delta^3 x} - \frac{3}{\delta^2 x^2} + \frac{3}{2\delta x^3}\right)\theta_n(x+\delta) +$$

$$\left(-\frac{4}{\delta^4} + \frac{6}{\delta^3 x} + \frac{3}{\delta^2 x^2} + \frac{3}{2\delta x^3}\right)\theta_n(x-\delta) + \left(\frac{1}{\delta^4} + \frac{3}{\delta^3 x}\right)\theta_n(x+2\delta) +$$

$$\left(\frac{1}{\delta^4} - \frac{3}{\delta^3 x}\right)\theta_n(x-2\delta) = 16\bar{F}_n(x) \quad (38)$$

The desirable boundary conditions for θ_n are the ones which give a smooth solution. For the tapered-beam analogy of equation (30) the obvious boundary conditions meeting these requirements are those representing unsupported ends. When these boundary conditions are transformed in terms of the variable x they become

$$\left.\begin{aligned} &\text{at } x = 0, \quad \frac{d\theta_n}{dx} = \frac{d^3\theta_n}{dx^3} = 0 \\ &\text{at } x = 1, \quad \frac{d^2\theta_n}{dx^2} = \frac{d^3\theta_n}{dx^3} = 0 \end{aligned}\right\} \tag{39}$$

A first attempt to solve the finite-difference equations (39) by relaxation was unsuccessful because of slow and erratic convergence. Instead, Crout's method of solving simultaneous equations (ref. 10) was used to determine the values of θ_n at 11 points ($\delta = 0.10$) at once. This could be done rapidly, but unfortunately 11 points were not enough to determine accurately the end values and derivatives which were required. Instead of decreasing the spacing to 0.05 throughout, it was decided to add two end sections from 0 to 0.3 and from 0.7 to 1.0 with 0.05 spacing. The solutions in these end sections were joined with the original solution at the 0.30 and 0.70 stations where the function and its first derivative were matched. Since the higher derivatives were small at the junction points (especially for $\lambda = 4$ and 7) this method was adequate, but did cause some trouble when higher derivatives were required for the succeeding calculations.

Calculations of θ_2 were made for $\lambda = 4$, 7, 10, and 13, while for $\lambda = 4$ and 7 the calculations were continued to determine θ_3 and θ_4. As λ increases convergence of the series for P deteriorates rapidly and the function θ_n has increasingly large oscillations. It was decided therefore not to continue the calculations for $\lambda = 10$ and 13. The values of p_n obtained are shown in table 4, while the values of w_n and f_n are shown in tables 2 and 3 and plotted in figures 9 and 10.

For $\lambda = 4$ the convergence of the series for p_n was very satisfactory, the contribution of the fourth-order term still being small at the critical buckling load. In figure 11 is shown a plot of load P versus the center deflection ratio W_o and in figure 12 are shown the deflection modes for several values of the center deflection ratio W_o. These deflection modes have their maximum at the center, and as W_o grows they become increasingly peaked toward the center.

For $\lambda = 7$, however, the convergence is poor and the coefficients p_n all being positive, no buckling can be determined using just four terms.

The convergence is good enough to determine the deflection shapes W for small values of W_o and these are plotted in figure 12. These deflection shapes give an explanation of why p_2 is positive (which implies increasing stiffness with respect to the center deflection as the load increases) since they show that the maximum deflection is no longer at the center and that with increasing load the center deflection becomes a progressively small portion of the maximum deflection. This characteristic is corroborated by the experimental measurements.

The deflection modes for $\lambda = 10$, which are also shown in figure 12, exhibit the same characteristic, but with the position of the maximum deflection moved outward toward the edge. However, since these curves are calculated using only two terms of the expansion for W, these curves should not be taken as indicating accurately what happens at the larger values of W_o.

The rapid change which must occur at buckling from a shape in which the maximum deflection occurs near the edge to one in which the maximum deflection occurs at the center is probably also an explanation for the poor convergence. Since the experimental results show that at $\lambda = 10$ the maximum deflection is again at the center it may be that for these higher values of λ the convergence is actually improved. However, to obtain accurate values of θ_n for these higher values of λ it would be necessary to start with a smaller finite-difference interval than was used here.

Since the influence of the p_3 and p_4 terms at the buckling load for $\lambda = 4$ was small, it was felt that for $\lambda < 5$ an adequate approximation to the buckling load could be obtained using just the first two terms p_1 and p_2. The critical conditions occur when $\frac{dP}{dW_o} = 0$ so that for

$$P = p_1 W_o + p_2 W_o^2$$

the critical conditions are

$$\left.\begin{aligned} W_{o_{cr}} &= \frac{-p_1}{2p_2} \\ P_{cr} &= \frac{-p_1^2}{4p_2} \end{aligned}\right\} \tag{40}$$

This value of P_{cr} is plotted in figure 13 where it is compared with the experimental results. The minimum value of λ for which P_{cr} exists is that for which the critical deflection equals the initial height of the dome, that is, for $W_{o_{cr}} = h/t$.

EXPERIMENTAL PROGRAM

Equipment

An experimental program was carried out on a series of shallow domes having a base diameter of 8 inches, nominal radii of curvature of 20 and 30 inches, and nominal thicknesses varying from 0.032 to 0.102 inch. The edges of the specimens were held between two rings which were bolted to a circular plate (figs. 14 and 15) thus providing a rigid built-in edge support and a closed pressure chamber. A separate set of clamping rings was used for each of the two radii of curvature. The specimens were subjected to a uniform normal load using both oil and air pressure; the oil provided an approximation to a constant volume characteristic during buckling while the air provided a constant pressure characteristic.

The specimens were made by spinning from flat sheet. After unsuccessful attempts to heat-treat aluminum spinnings, magnesium alloy QQ-M-44 was selected because of its favorable ratio of yield stress to Young's modulus compared with other non-heat-treated metals. Magnesium also has the advantage that since it is spun while hot most of the residual stresses are eliminated. This is evidenced by the small separation when a radial cut is made in a magnesium spinning. Because of the difficulty of spinning such shallow shells the preliminary specimens were very disappointing, but by a combination of spinning on concave and convex molds the quality was greatly improved. Unfortunately it is still not so good as would be desired.

Pressure measurements were made using a Bourdon tube for pressure over 20 psi and a mercury manometer for pressures under 20 psi. Exceptions were two of the early specimens having low buckling loads which were tested using the Bourdon gage. This gage of course gives a closer approximation to a constant volume characteristic than does the manometer.

Deflection measurements were taken with a 0.001-inch-scale dial gage riding on a channel beam fastened at its ends to a circular ring which rotated in a groove cut in the upper clamping ring. Readings were made to the nearest 0.0005 inch. Traverses were made on two or more diameters to determine the initial shape of the shell and were repeated at intervals during the loading. Intermediate measurements were also made of the center deflection. Because of the variations of the specimens from a true spherical form the question arose as to what should be taken as the

radius R from which the parameter λ was calculated. It was decided to assume that the central rise h would determine the radius since λ can be simply expressed in terms of h (eqs. (21)) and because experience with the buckling of shallow arches showed that for arches having the same central height small symmetrical variations in shape have only a small effect on the buckling load. In figure 16 the variations from the assumed radii are shown for typical examples of each of the six combinations of the two nominal radii, 20 and 30 inches, and each nominal initial sheet thickness 0.032, 0.054, and 0.102. It is seen that the variations increased markedly with the thinness of the sheet and the flatness of the dome.

Oil Tests

The oil pressure tests were made first, and two or more tests of each combination of thickness and radius were made. The early preliminary tests made on aluminum samples all showed a very distinct unsymmetrical buckling mode. This is believed due to the high residual stresses resulting from the spinning operation since the majority of the magnesium specimens buckled symmetrically. In the cases in which unsymmetrical buckle did occur in the magnesium specimens the mode was not of the overall unsymmetrical form such as the unsymmetrical mode of vibration of a flat circular plate. Rather it appeared that the buckles themselves were inherently symmetrical but were displaced from a central position on the shell, probably because of initial asymmetries of the shell.

The unsymmetrical buckling occurred only in the range of λ between 6.0 and 8.6 and was associated with a prebuckling deflection mode in which the displacement at about half the radius from the center was greater than that at the center.

In figure 16 are shown the deflection curves of the specimens. There is a distinct change in the deflection modes as λ increases. For λ near 4 the deflection is peaked at the center and decreases steadily toward the edge. As λ increases, the peak gradually flattens out, until at $\lambda = 5.45$ the maximum deflection no longer occurs at the center. Instead, at large deflections there are two peaks symmetrically placed at about a half radius from the center. With a further increase in λ the peaks move outward until finally when $\lambda = 8.98$ a third peak appears in the center. This gradually becomes the predominant peak. These trends agree very well with the theoretical deflection curves for $\lambda = 4$, 7, and 10 shown in figure 12.

In figures 11 and 17 are plotted the curves of pressure versus center deflection of the specimens. For low values of λ ($\lambda < 5$), the specimens buckled in a continuous manner. As more oil was pumped into the chamber the pressure increased more slowly, reached a maximum, and

then decreased. But for $\lambda > 5$, the process was discontinuous. Usually there would be a slight movement of the shell without the addition of oil followed by a sudden jump to a lower pressure and a greater displacement. There was no regular trend in the ratio of the pressure after buckling $\left(P_{cr}\right)_2$ to the buckling pressure P_{cr} as λ increased and also surprisingly no significant difference in this ratio between the tests made using the Bourdon tube and those using the manometer.

Air Pressure Tests

For the air pressure tests an accumulator tank was connected to the air line close to the testing fixture so that the buckling process was practically a constant pressure process. Buckling occurred very suddenly and with a sharp report. The final buckled shapes were symmetrical with deflections very much larger than those of the oil tests. Deflection traverses were made during loading, but it was inadvisable to make them at loads approaching the expected buckling load. Two examples of these deflection traverses are shown in figures 16(g) and 16(h).

The specimens remained in their buckled position after the pressure was released. An approximate determination of the pressure required to unbuckle them was made by unbolting the clamping rings, inverting the rings with the specimens still placed between them, and then bolting the inverted assembly to the base plate. The pressures required to unbuckle the specimens were considerable and are included in table 5.

DISCUSSION

The physical parameters and buckling loads of all the specimens are shown in table 5. In figure 18 are plotted the buckling loads as a function of λ. The oil pressure tests are shown with black dots, while the air tests are shown with open circles. For the oil tests the points at the lower ends of the dashed lines indicate the value to which the pressure jumped during the buckling process, while a wing on the left of a lower circle indicates an unsymmetrical buckling mode. When plotted on logarithmic paper the results tended to follow two intersecting lines. In figure 18 the corresponding power-law curves are shown.

In figure 13 the experimental buckling loads are compared with the theoretical loads calculated using two terms of the series for $\lambda < 5$, and the one point calculated using four terms for $\lambda = 4$. In figure 11 the corresponding curves of load versus center deflection are also compared. Although the experimental results are low compared with the theory, the difference (approximately 15 percent at $\lambda = 4$) is not great

considering the variations of the initial shapes from a true spherical surface. Part of the difference can be attributed to yielding which occurred at the higher loads, especially for the specimens having values of λ near 5. It is felt that the results are close enough to corroborate the theory proposed and establish the applicability of the classical criterion for buckling for the lower range of λ ($\lambda < 5$).

From figure 18 it is clear that the type of loading, air or oil, has little if any effect on the buckling load. This is expected to be the case if the classical buckling criterion holds, but would be rather unexpected if Tsien's "energy criterion" applied. For in Tsien's theory when the buckled and unbuckled energy levels are compared the loss in potential energy of the load during buckling must be included. Since the loss in potential energy is a maximum when the pressure remains constant, the buckling in a constant-pressure system should occur at a lower load than for any system in which the pressure decreases during buckling. Rather large differences in the buckling loads between a "rigid testing machine" (approximated by oil loading) and a "dead-weight loading" (approximated by air pressure loading) are predicted by Tsien in reference 6, according to the energy criterion, for complete spheres and also for spherical domes of fairly large values of λ. As remarked before, however, the calculations as given in reference 6 are probably inapplicable to domes as shallow as those tested here, and a more accurate energy expression and deflection mode should be used. Although it is impertinent to reject the energy criterion on the basis of the disappearance of the difference in buckling loads between the rigid testing machine and dead-weight loading, the fact that the buckling loads given by the classical criterion are reasonably close to the experimental values for $\lambda < 5$ seems to indicate that, at such small values of λ, a refinement of the energy-criterion calculations is unwarranted.

The buckling stress for spherical shells is usually expressed in the form

$$\sigma_{cr} = KE\frac{t}{R} \qquad \left(\sigma_{cr} = \frac{R}{2t}q_{cr}\right) \qquad (41)$$

where K is a numerical constant. The classical theory for the buckling of complete spheres gives a value of K of order 0.606 with $\mu = 0.3$ (see eq. (2)). Tsien's theory in reference 6 gives a K of order about half of that given by the classical theory. The calculation based on the classical criterion given in this paper, for very shallow domes, also gives a value of K ranging from 0.2 to 0.4. Both reference 6 and the present paper predict K as a function of the parameter λ. A composite picture showing the results of all available theoretical and experimental data is given in figure 19, where K is plotted against the parameter λ. It is to be remarked again that all the curves labeled "Theory" should

be read with caution. On the extreme left, the theoretical result according to equation (40) does not converge for values of $\lambda > 5$, and extrapolation to larger λ values is dangerous. On the other hand, the curve showing theoretical results of reference 6 probably is good only toward the right-hand end; the left-hand end of that curve probably should be more carefully computed. In other words, to do justice to either the classical criterion of buckling or the energy criterion of buckling, both theoretical curves shown in figure 19 should be recalculated to higher accuracy. The curve showing the "classical linear theory" applies only to complete spheres and is shown here for reference.

Even though not proved rigorously, a trend of shifting from the classical criterion to the energy criterion at λ of order 6 seems to be indicated by the experimental results. This transitional value of λ is probably low on account of the imperfections of the test specimens.

A comparison of the above results with the case of low arches as given in reference 7 reveals a fundamental difference, with respect to the stability criteria, between the buckling under lateral forces of a spherical dome and an arch. In the arch case the classical criterion holds for larger values of λ (i.e., higher arches), and a transition to the energy criterion occurs as the arch becomes very low. In the dome case the classical criterion holds for smaller values of λ (i.e., very shallow domes), and a transition to the energy criterion occurs as the dome becomes higher.

SUMMARY OF RESULTS

In this paper an attack upon the problem of the finite deflection of a shallow spherical shell has been made. The results may be summarized as follows:

1. The theoretical approach has been to transform the nonlinear equations into a sequence of linear equations by expanding all the unknown functions in powers of the nondimensional center deflection W_o and equating coefficients of equal powers of W_o. The initial linear equation can be solved exactly in terms of the ber and bei functions, but the succeeding equations have had to be solved either by power series or numerical methods. For small values of the parameter λ the resulting series converges rapidly enough so that a determination of the buckling load can be made using only four terms of the series. For higher values of λ the convergence deteriorates rapidly, so that for λ greater than 5 no determination of the buckling load can be made. However, for deflections smaller than the critical buckling deflection, the deflection modes can be determined for a much wider range of λ. These deflection modes change rapidly with λ and for values of λ near 7 have the surprising

characteristic that the maximum deflection occurs approximately halfway between the center and the edge of the shell.

2. For small values of λ the results of the experimental program agreed substantially with those of the theoretical analysis. The buckling load near $\lambda = 4$ was only about 15 percent below the theoretical value while the trend of the buckling loads as λ increased was approximately the same as predicted by the theory. The deflection modes also showed the same characteristics as predicted by the theory. The experimental buckling mode was inherently symmetrical as assumed in the theory; the few exceptions can be attributed to large initial asymmetries in the specimens.

3. Tests were made with both air and oil pressure, which approached the extremes of constant pressure and constant volume buckling characteristics, respectively. The buckling loads obtained by the two methods showed no significant difference; thus a feature of the "energy criterion" did not appear.

4. Experimental results seem to indicate that the classical criterion of buckling is applicable to very shallow spherical domes and that a transition to energy criterion occurs for higher domes.

California Institute of Technology,
Pasadena, Calif., August 13, 1953.

APPENDIX A

INFINITE-SERIES EXPANSION

After substituting the expressions for f_n and w_n, equation (33), into the second of equations (28) for F_2, it becomes

$$F_2 = \frac{3}{8}\frac{p_1 k}{x}(A_1\,\mathrm{bei}'\lambda x - B_1\,\mathrm{ber}'\lambda x) - \frac{k^2\lambda^2}{16x^2}\left\{A_1B_1\left[(\mathrm{bei}'\lambda x)^2 - (\mathrm{ber}'\lambda x)^2\right] + \left(A_1^2 - B_1^2\right)\mathrm{ber}'\lambda x\,\mathrm{bei}\,\lambda x\right\} - \frac{k^2}{32x^2}\left(\frac{d^2}{dx^2} - \frac{1}{x}\frac{d}{dx}\right)\left(A_1\,\mathrm{bei}\,\lambda x - B_1\,\mathrm{ber}'\lambda x\right)^2 \tag{A1}$$

The particular integral of equation (26a) corresponding to the first term of equation (A1) is

$$\theta_2' = -\frac{3}{2}\frac{p_1 k}{\lambda^3}\left(A_1\,\mathrm{bei}'\lambda x - B_1\,\mathrm{ber}'\lambda x\right) \tag{A2}$$

The particular integral for the remaining terms of F_2 (all quadratic in ber' and bei') is obtained by expanding in series. The series expansions for $\mathrm{ber}'\lambda x$ and $\mathrm{bei}'\lambda x$ are

$$\left.\begin{aligned}\mathrm{ber}'\lambda x &= \sum_{n=1}^{} (-)^n \frac{\left(\frac{1}{2}\lambda x\right)^{4n-1}}{(2n-1)!(2n)!}\\ \mathrm{bei}'\lambda x &= \sum_{n=0}^{} (-)^n \frac{\left(\frac{1}{2}\lambda x\right)^{4n+1}}{(2n)!(2n+1)!}\end{aligned}\right\} \tag{A3}$$

In terms of the above series the expansion of the quadratic terms of F_2 becomes.

$$F_2'' = -\frac{k^2\lambda^2}{64}\left\{A_1B_1\left[a_n + b_n + 2(n+1)(2n+1)C_{n+1}\right]\left(\frac{\lambda x}{2}\right)^{4n} + \left[\left(A_1^2 - B_1^2\right)C_n + n(2n+1)\left(A_1^2a_n - B_1^2b_n\right)\right]\left(\frac{\lambda x}{2}\right)^{4n-2}\right\} \tag{A4}$$

where

$$\left.\begin{aligned} a_n &= (-)^n \sum_{m=0} \frac{1}{(2n-2m)!(2n-2m+1)!(2m)!(2m+1)!} \\ b_n &= (-)^n \sum_{m=1} \frac{1}{(2n-2m+1)!(2n-2m+2)!(2m-1)!(2m)!} \\ c_n &= (-)^n \sum_{m=1} \frac{1}{(2n-2m)!(2n-m+1)!(m-1)!m!} \end{aligned}\right\} \tag{A5}$$

The corresponding particular integral of equation (26a) is

$$\theta_2'' = \frac{1}{4}k^2 \sum_{n=0}\left[A_1B_1d_n\left(\frac{\lambda x}{2}\right)^{4n} + \left(A_1^2g_n + B_1^2h_n\right)\left(\frac{\lambda x}{2}\right)^{4n-2}\right] \tag{A6}$$

where

$$\left.\begin{aligned} d_n &= \frac{1}{4n^2\left(4n^2-1\right)}\left[2n(2n-1)C_n - a_{n-1} - b_{n-1} - d_{n-1}\right] && n \geqq 1 \\ g_n &= \frac{-1}{(2n-1)^2\left[(2n-1)^2-1\right]}\left[(n-1)(2n-1)a_{n-1} + c_{n-1} + g_{n-1}\right] && n \geqq 2 \\ h_n &= \frac{1}{(2n-1)^2\left[(2n-1)^2-1\right]}\left\{(n-1)(2n-1)b_{n-1} + c_{n-1} - h_{n-1}\right\} && n \geqq 2 \\ g_o &= h_o = 0 \end{aligned}\right\} \tag{A7}$$

The values of d_o, g_1, and h_1 are arbitrary with respect to the recursion formula of the differential equation, but when equation (A6) is combined with equation (A2) it is required that

$$\left.\begin{aligned} d_o &= \frac{1}{2} \\ h_1 &= \frac{1}{2} \end{aligned}\right\} \tag{A8}$$

in order that $\theta_2 = \theta_2' + \theta_2''$ have the proper limiting value as $\lambda \longrightarrow 0$.

The coefficient g_1 is completely arbitrary and for convenience was taken as equaling unity.

The infinite-series expansion for φ_2 is

$$\varphi_2 = \sum_{n=0} \left[\frac{A_1^2 a_n - B_1^2 b_n}{4n+2} \left(\frac{\lambda - x}{2} \right)^{4n+2} - A_1 B_1 \frac{C_n}{2n} \left(\frac{\lambda x}{2} \right)^{4n} \right] \tag{A9}$$

Then θ_2 and its derivatives and φ_2 are substituted in equations (35) to determine α_n and β_n which are in turn substituted into the boundary conditions, equations (34), to obtain A_2, B_2, and p_2.

REFERENCES

1. Timoshenko, S.: Theory of Plates and Shells. First ed., McGraw-Hill Book Co., Inc., 1940.

2. Timoshenko, S.: Theory of Elastic Stability. First ed., McGraw-Hill Book Co., Inc., 1936.

3. Reissner, E.: Stresses and Small Displacements of Shallow Spherical Shells, (I). Jour. Math. and Phys., vol. 25, 1946, pp. 80-85; (II). Jour. Math. and Phys., vol. 25, 1947, pp. 279-300.

4. Von Kármán, Th., and Tsien, Hsue-Shen: The Buckling of Spherical Shells by External Pressure. Jour. Aero. Sci., vol. 7, no. 2, Dec. 1939, pp. 43-50.

5. Friedrichs, K. O.: On the Minimum Buckling Load for Spherical Shells. Theodore von Kármán Anniversary Volume, C.I.T. (Pasadena), 1941, pp. 258-272.

6. Tsien, Hsue-Shen: A Theory for the Buckling of Thin Shells. Jour. Aero. Sci., vol. 9, no. 10, Aug. 1942, pp. 373-384.

7. Fung, Y. C., and Kaplan, A.: Buckling of Low Arches or Curved Beams of Small Curvature. NACA TN 2840, 1952.

8. Biezeno, C. B.: Über die Bestimmung der "Durchschlagkräft" einer schwachgekrümmten, Kreisförmigen Platte. Z.a.M.M., Bd. 15, 1935, pp. 10-22. (This is reproduced in the book Technische Dynamik, by C. B. Biezeno and R. Grammel, Julius Springer (Berlin), 1939.)

9. Chien, W. Z.: Large Deflection of a Circular Clamped Plate Under Uniform Pressure. Chinese Jour. Phys., vol. VII, no. 2, Dec. 1947, pp. 102-113.

10. Milne, W. E.: Numerical Calculus. Princeton Univ. Press (Princeton), 1949, ch. 1.

TABLE 1

VALUES OF A_1, B_1, AND p_1

λ	A_1	B_1	p_1
0.5	-4.875	155.9	5.333
.7	-3.481	56.78	5.361
1.0	-2.434	19.39	5.441
1.5	-1.614	5.614	5.877
2.0	-1.194	2.200	7.061
3.0	-.7298	.4093	14.35
4.0	-.4275	-.06698	35.97
5.0	-.1835	-.2078	89.55
6.0	-.005114	-.1892	206.2
7.0	.07882	-.09905	426.1
8.0	.07857	-.01571	784.7
9.0	.4214	-.02332	1,311
10.0	.009895	.02615	2,043
11.0	-.005344	.01498	3,031
12.0	-.007743	.004468	4,343
13.0	-.004895	-.0009003	6,048
14.0	-.001736	-.002132	8,219
15.0	-.00003355	-.001506	10,932

TABLE 2

VALUES OF w_n FOR $\lambda = 4, 7, 10,$ AND 13

x	$\lambda = 4$				$\lambda = 7$				$\lambda = 10$		$\lambda = 13$
	w_1	w_2	w_3	w_4	w_1	w_2	w_3	w_4	w_1	w_2	w_1
0	1.0000	0	0	0	1.000	0	0	0	1.000	0	1.0000
.05	.9965	-.0021	-.0018	-.0008	1.0011	.0080	.020	.052	1.0002	-.0014	.9999
.10	.9859	-.0082	-.0072	-.0032	1.0044	.032	.079	.206	1.0010	-.0053	.9995
.15	.9683	-.0181	-.016	-.0068	1.0093	.070	.173	.453	1.0025	-.0091	.9988
.20	.9436	-.0312	-.027	-.011	1.0152	.121	.300	.782	1.0053	-.011	.9979
.25	.9116	-.0470	-.039	-.015	1.0211	.182	.449	1.173	1.0099	-.018	.9970
.30	.8724	-.065	-.051	-.019	1.0254	.250	.614	1.604	1.0168	.017	.9964
.40	.7725	-.101	-.073	-.023	1.0214	.386	.938	2.435	1.0381	.112	.9993
.50	.6453	-.130	-.081	-.019	.9825	.477	1.141	2.952	1.0625	.300	1.0148
.60	.4958	-.141	-.074	-.0092	.8832	.480	1.129	2.903	1.0608	.517	1.0438
.70	.3338	-.126	-.053	.0006	.7016	.366	.863	2.187	.9708	.614	1.0437
.75	.2533	-.110	-.039	.0034	.5787	.289	.684	1.777	.8672	.581	.9955
.80	.1769	-.087	-.025	.0037	.4391	.191	.473	1.242	.7149	.463	.8851
.85	.1085	-.059	-.013	.0031	.2920	.106	.280	.740	.5169	.306	.6945
.90	.0525	-.032	-.0048	.0018	.1528	.040	.127	.348	.2938	.139	.4290
.95	.0143	-.0087	-.0011	.0052	.0448	.0087	.032	.089	.0931	.034	.2960
1.00	0	0	0	0	0	0	0	0	0	0	0

TABLE 3

VALUES OF f_n FOR $\lambda = 4, 7, 10$, AND 13

x	$\lambda = 4$				$\lambda = 7$				$\lambda = 10$	$\lambda = 13$
	f_1	f_2	f_3	f_4	f_1	f_2	f_3	f_4	f_1	f_1
0	-4.244	1.353	0.180	0.0788	-16.246	-2.038	-7.04	-17.56	-37.21	-65.43
.05	-4.240	1.354	.180	.0781	-16.250	-2.069	-7.11	-17.77	-37.21	-65.43
.10	-4.227	1.358	.183	.0760	-16.262	-2.159	-7.34	-18.38	-37.22	-65.42
.15	-4.206	1.364	.186	.0724	-16.282	-2.305	-7.71	-19.38	-37.23	-65.41
.20	-4.176	1.372	.191	.0675	-16.306	-2.504	-8.21	-20.72	-37.25	-65.40
.25	-4.137	1.381	.196	.0612	-16.334	-2.749	-8.82	-22.36	-37.27	-65.39
.30	-4.089	1.391	.200	.0538	-16.360	-3.030	-9.52	-24.23	-37.32	-65.37
.40	-3.968	1.409	.207	.0361	-16.392	-3.670	-11.08	-28.39	-37.45	-65.37
.50	-3.811	1.418	.207	.0169	-16.353	-4.293	-12.54	-32.25	-37.64	-65.44
.60	-3.623	1.410	.198	-.0002	-16.178	-4.760	-13.58	-34.92	-37.82	-65.67
.70	-3.409	1.377	.184	-.0127	-15.795	-4.952	-13.92	-35.80	-37.76	-65.95
.75	-3.294	1.350	.176	-.0163	-15.507	-4.929	-13.83	-35.57	-37.54	-65.96
.80	-3.177	1.317	.167	-.0179	-15.153	-4.837	-13.58	-34.94	-37.12	-65.73
.85	-3.060	1.278	.159	-.0182	-14.737	-4.697	-13.22	-34.02	-36.46	-65.09
.90	-2.945	1.236	.152	-.0180	-14.271	-4.530	-12.79	-32.91	-35.56	-63.92
.95	-2.837	1.193	.146	-.0175	-13.780	-4.360	-12.33	-31.75	-37.46	-62.18
1.00	-2.737	1.153	.141	-.0170	-13.304	-4.206	-11.90	-30.65	-33.30	-60.12

TABLE 4

VALUES OF p_n $(n \geq 2)$ CALCULATED

λ	p_2		p_3	p_4
	Power series	Numerical		
1.0	-1.120			
1.5	-2.726			
2.0	-4.919			
3.0	-12.39			
4.0	-26.47	-26.5	3.77	1.08
5.0	-45.2			
6.0	-38.1			
7.0	53.7	56.6	314	801
8.0	219			
10.0		392		
13.0		537		

TABLE 5

EXPERIMENTAL DATA

$[\mu = 0.32, \quad E = 6.5 \times 10^6 \text{ psi}]$

(a) Hydraulic pressure tests

Specimen	t, in.	h, in.	λ	q_{cr}, psi	P_{cr}	Method of pressure measurement (a)	$(P_{cr})_2$
1	0.101	0.251	4.04	36.2	12.3	B	------
2	.099	.253	4.08	32.5	11.8	B	------
3	.101	.256	4.16	35.8	12.1	B	------
4	.100	.365	4.80	60.5	21.0	B	------
5	.101	.376	4.94	72.5	24.8	B	------
6	.053	.240	5.45	14.0	61.3	M	25.3
7	.053	.251	5.57	12.1	54.3	M	25.3
8	.052	.297	6.08	15.2	71.3	B	48.3
9	.055	.380	6.75	31	122.4	B	60.0
10	.051	.410	7.22	27.5	147	B	85.1
11	.051	.422	7.40	25.2	136	B	60.9
12	.031	.303	8.04	4.2	165	B	106
13	.032	.361	8.59	6.02	201	M	124
14	.031	.353	8.69	4.59	185	M	137
15	.033	.394	8.82	7.33	213	M	111
16	.033	.410	8.98	8.96	255	M	179
17	.029	.444	10.1	6.7	354	B	201

(b) Air pressure tests

Specimen	t, in.	h, in.	λ	q_{cr}, psi	P_{cr}	Pressure required to unbuckle specimen, psi
18	0.101	0.382	4.98	73.5	24.9	16.5
19	.101	.426	5.26	99.5	33.8	35
20	.055	.265	5.62	16.85	65.2	----
21	.054	.413	7.10	33.6	143	12.6
22	.032	.347	8.45	5.67	190	1.8
23	.033	.399	8.91	11.75	350	3.3

[a]B, Bourdon gage; M, manometer.

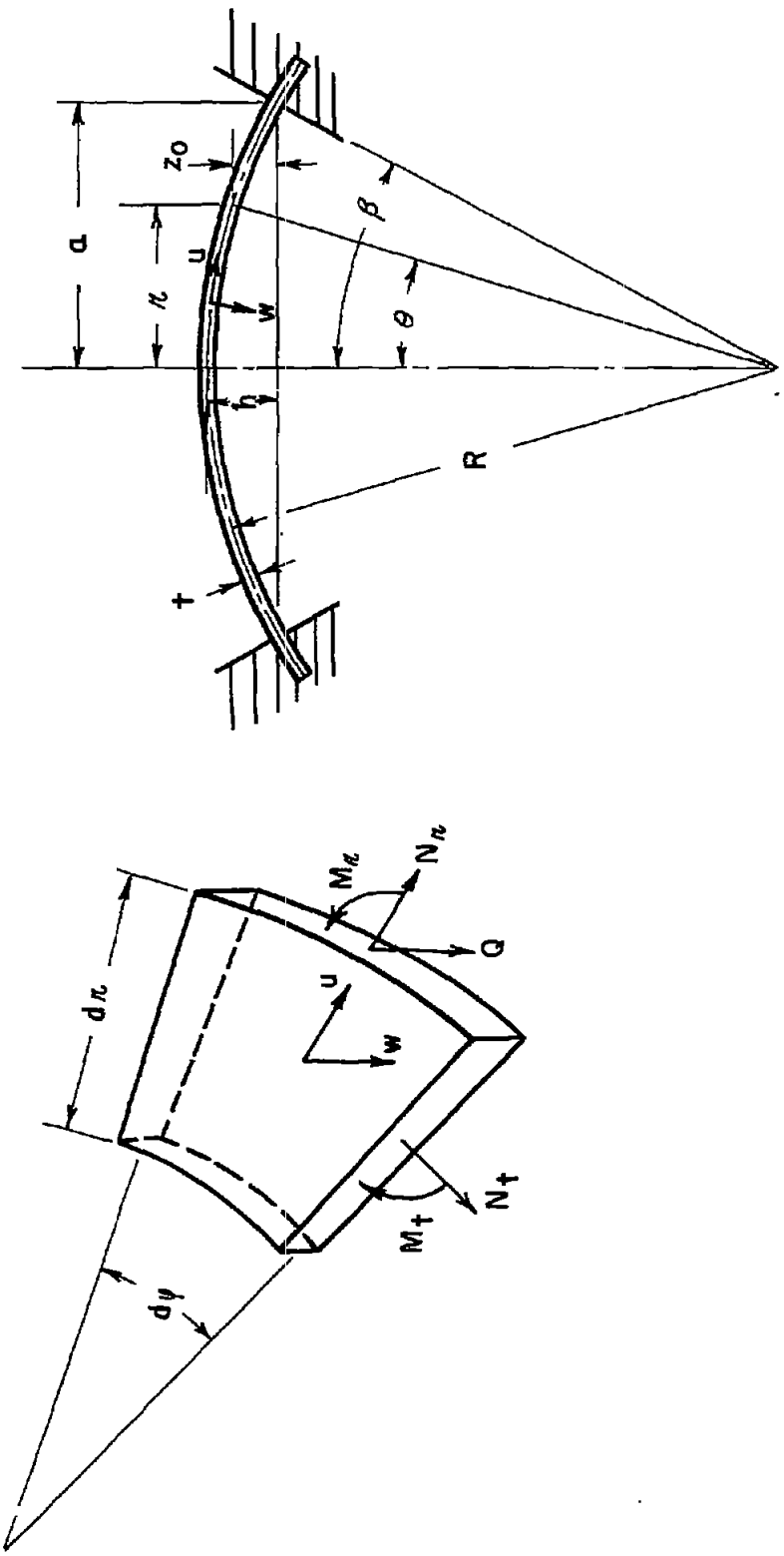

Figure 1.- Notation.

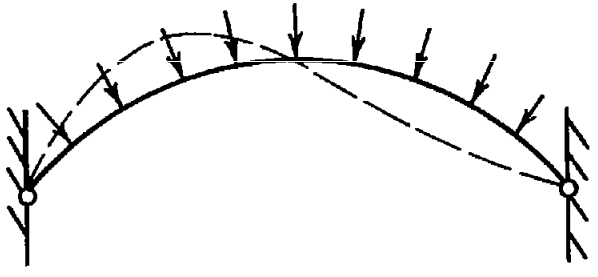

Figure 2.- Buckling mode for a high arch.

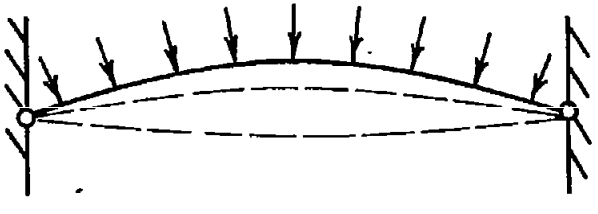

Figure 3.- Possible buckling mode of low arch.

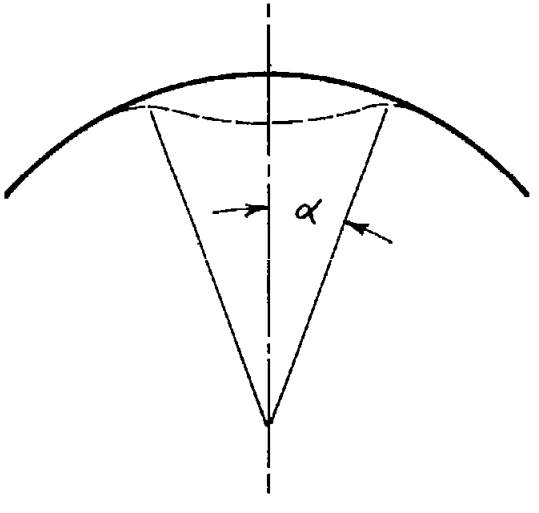

Figure 4.- "Applicable" and approximately "applicable" surfaces.

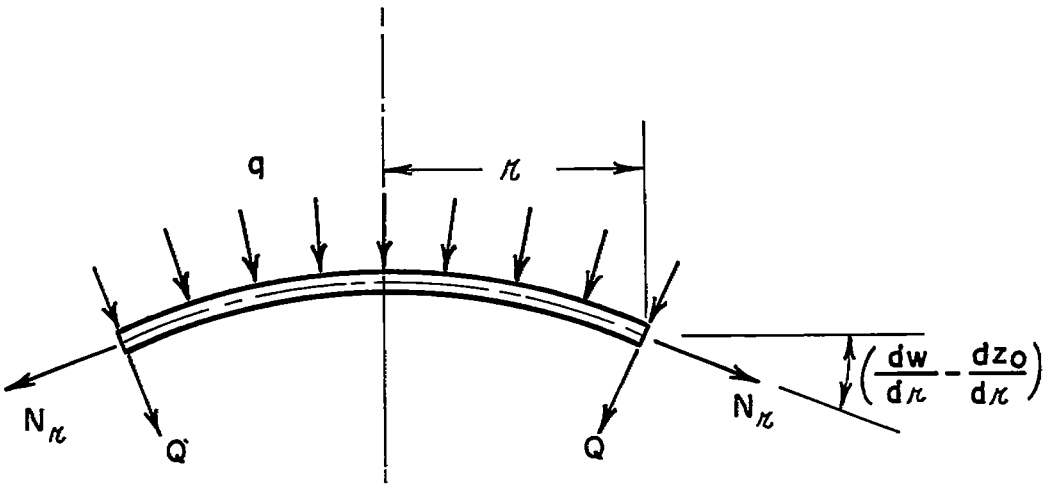

Figure 5.- Equilibrium of a central cylindrical section.

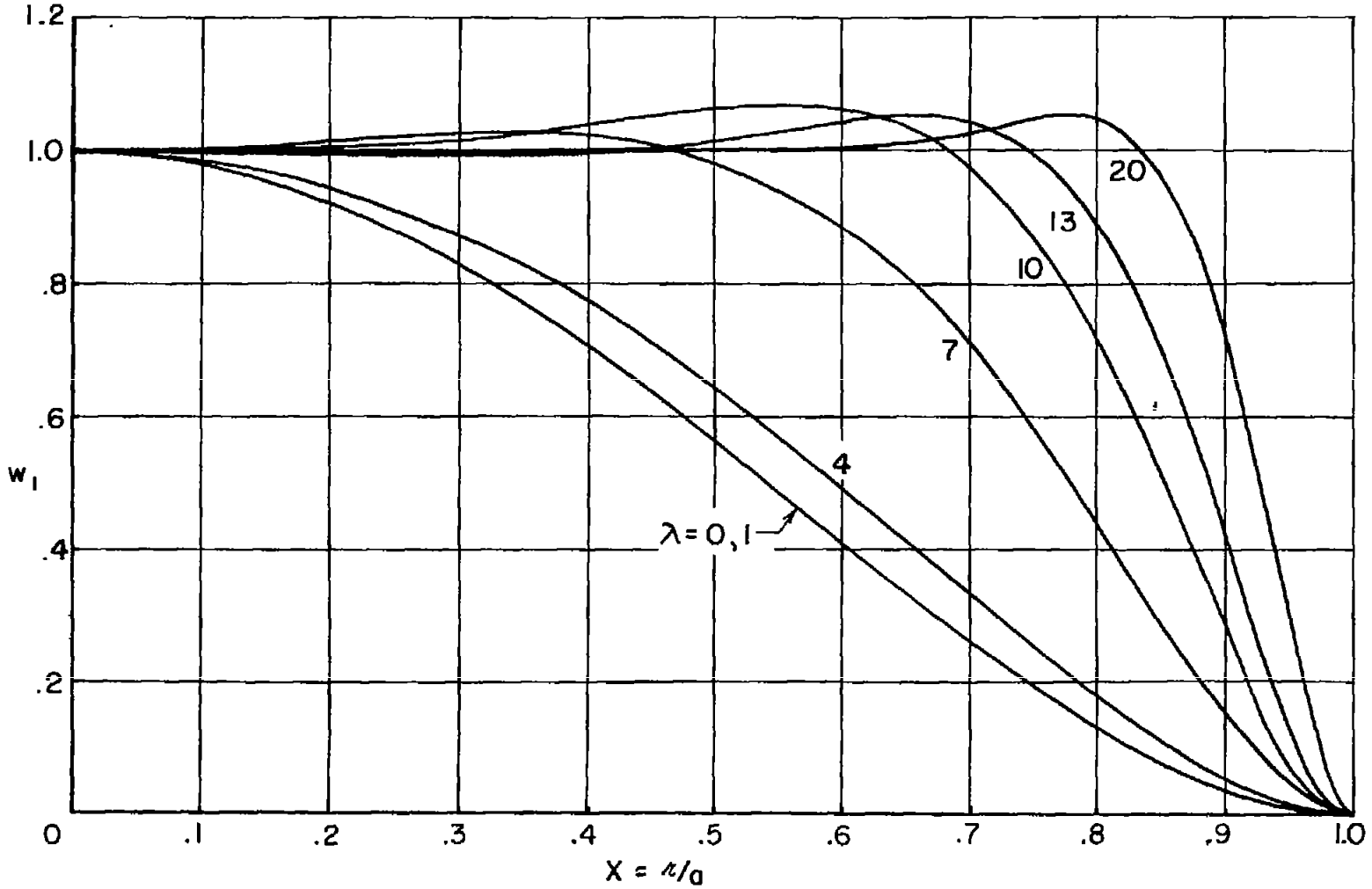

Figure 6.- Variation of linear deflection mode w_1 with λ.

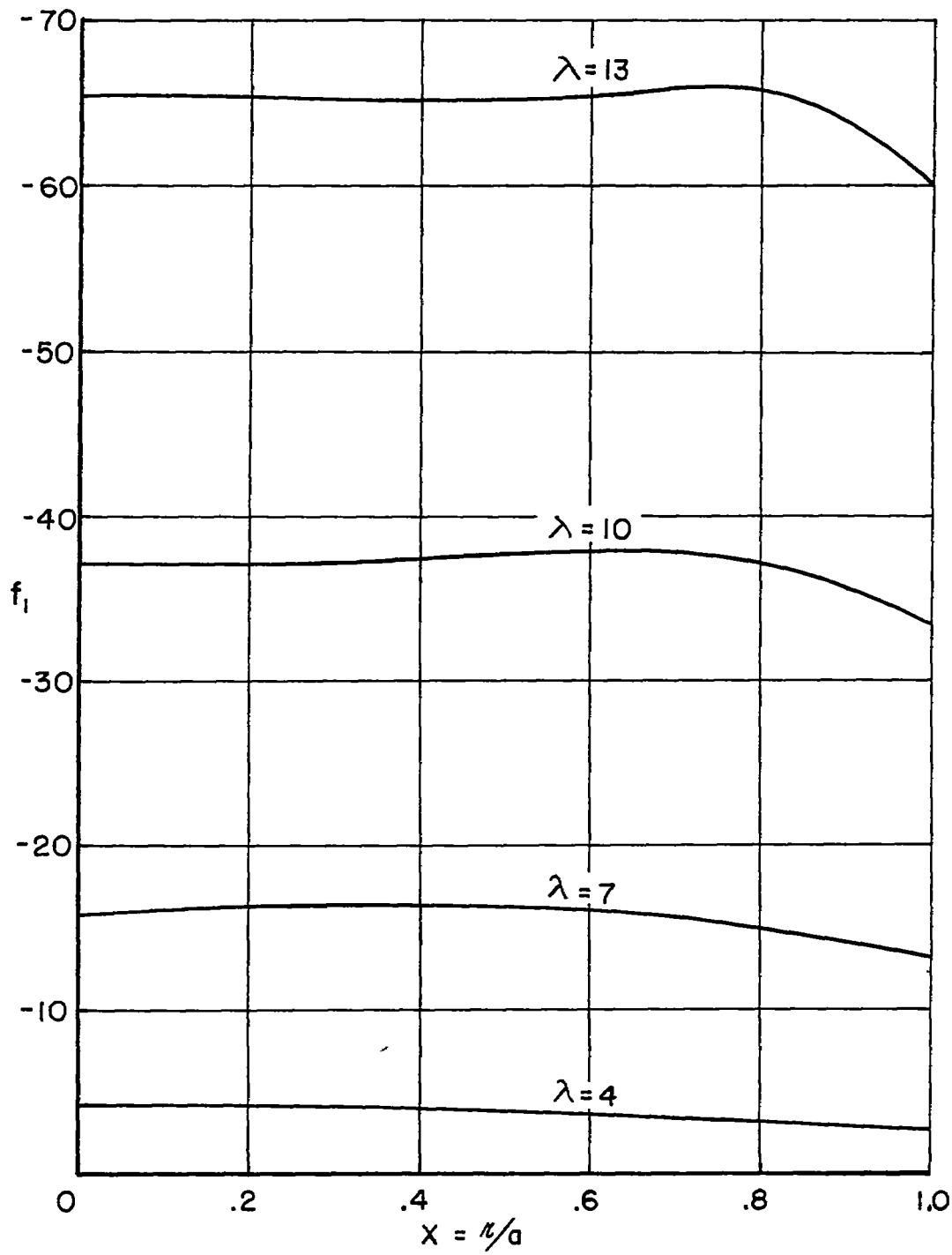

Figure 7.- Variation of linear membrane stress f_1 with λ.

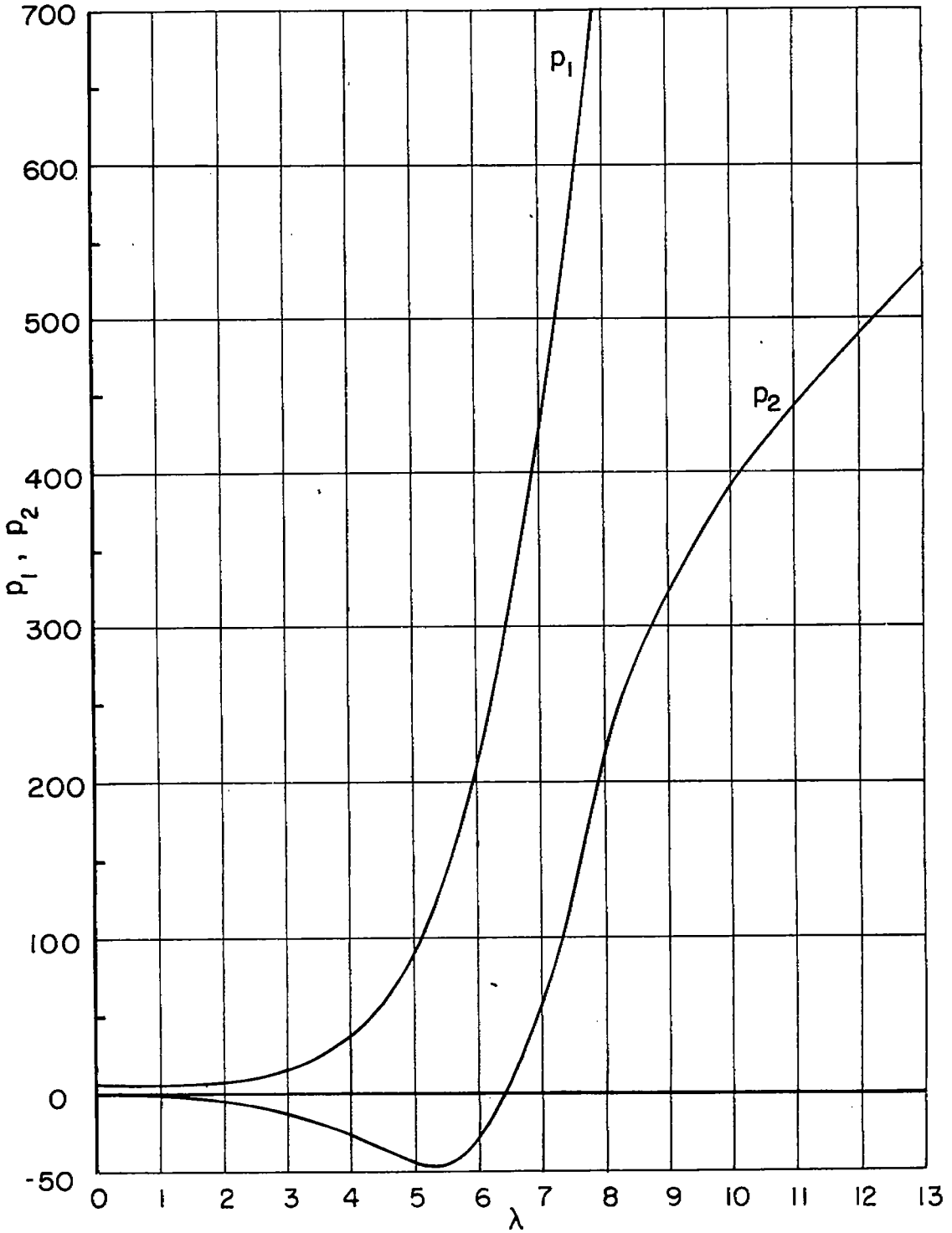

Figure 8.- Variation of p_1 and p_2 with λ.

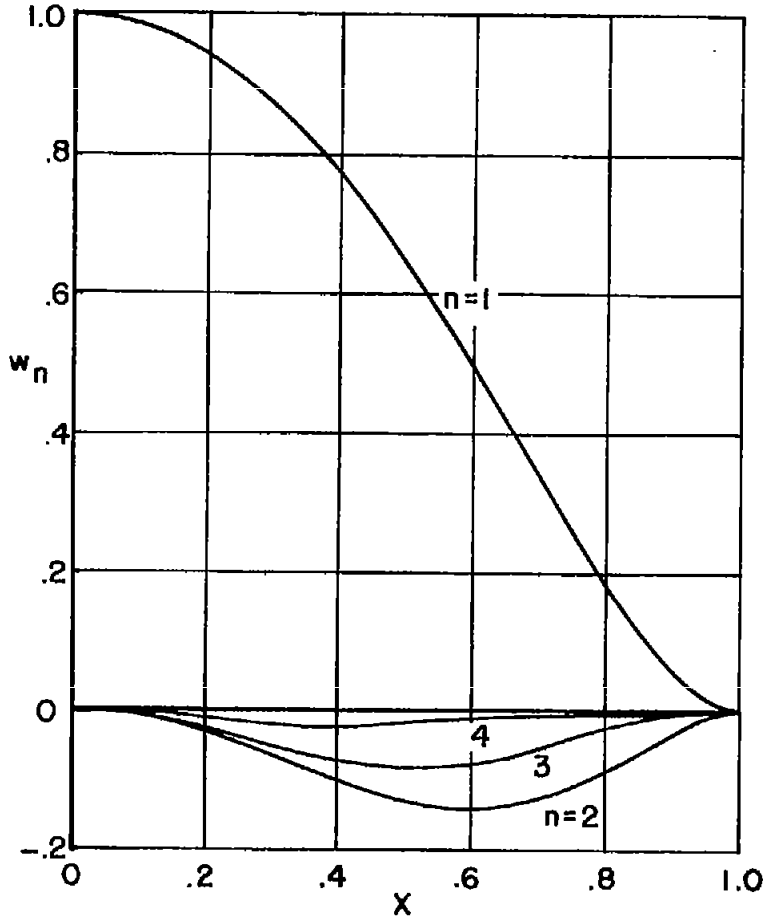

(a) $\lambda = 4$.

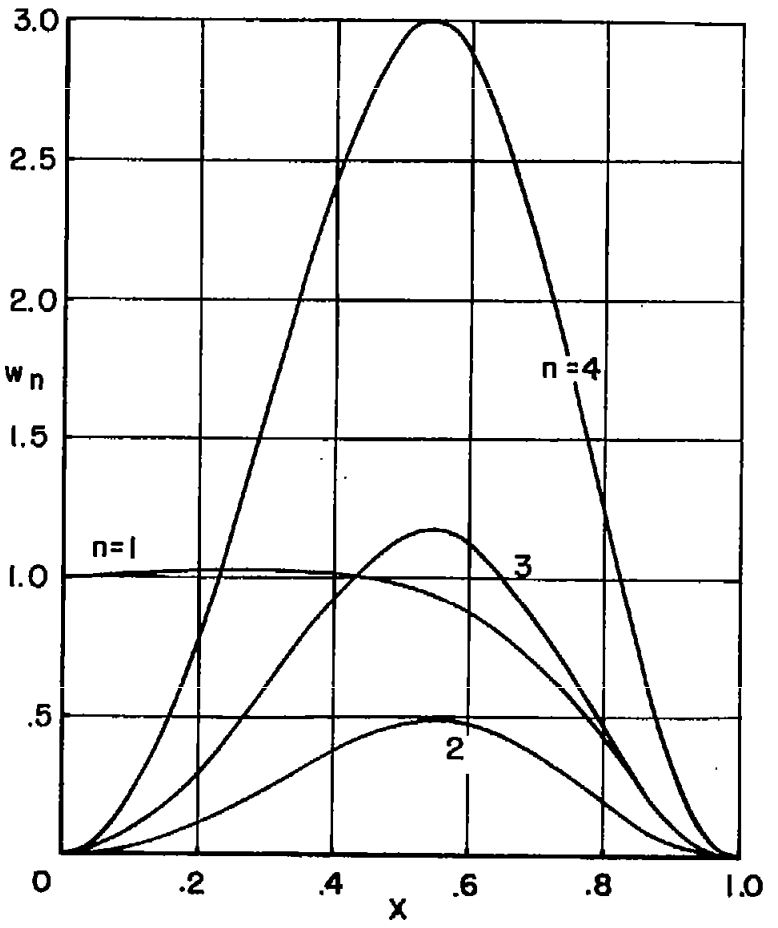

(b) $\lambda = 7$.

Figure 9.- First four terms of w_n for $\lambda = 4$ and 7.

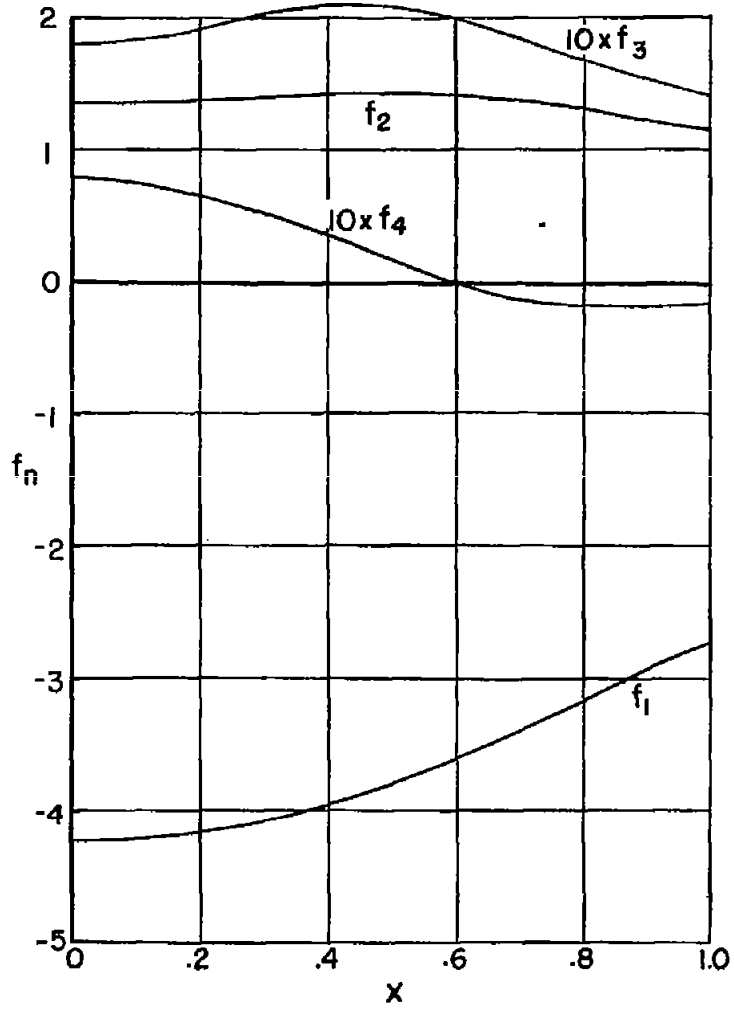

(a) $\lambda = 4$.

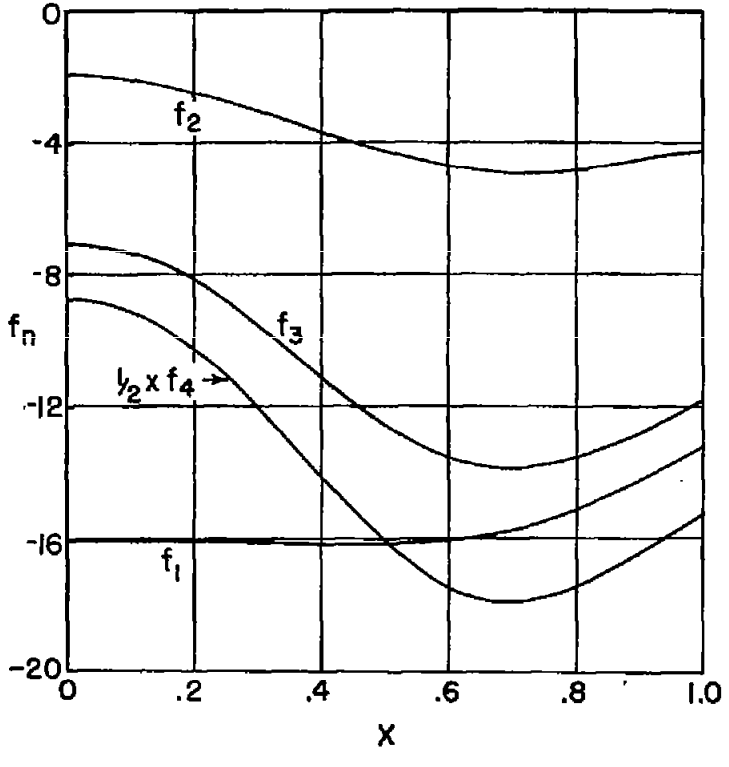

(b) $\lambda = 7$.

Figure 10.- First four terms of f_n for $\lambda = 4$ and 7.

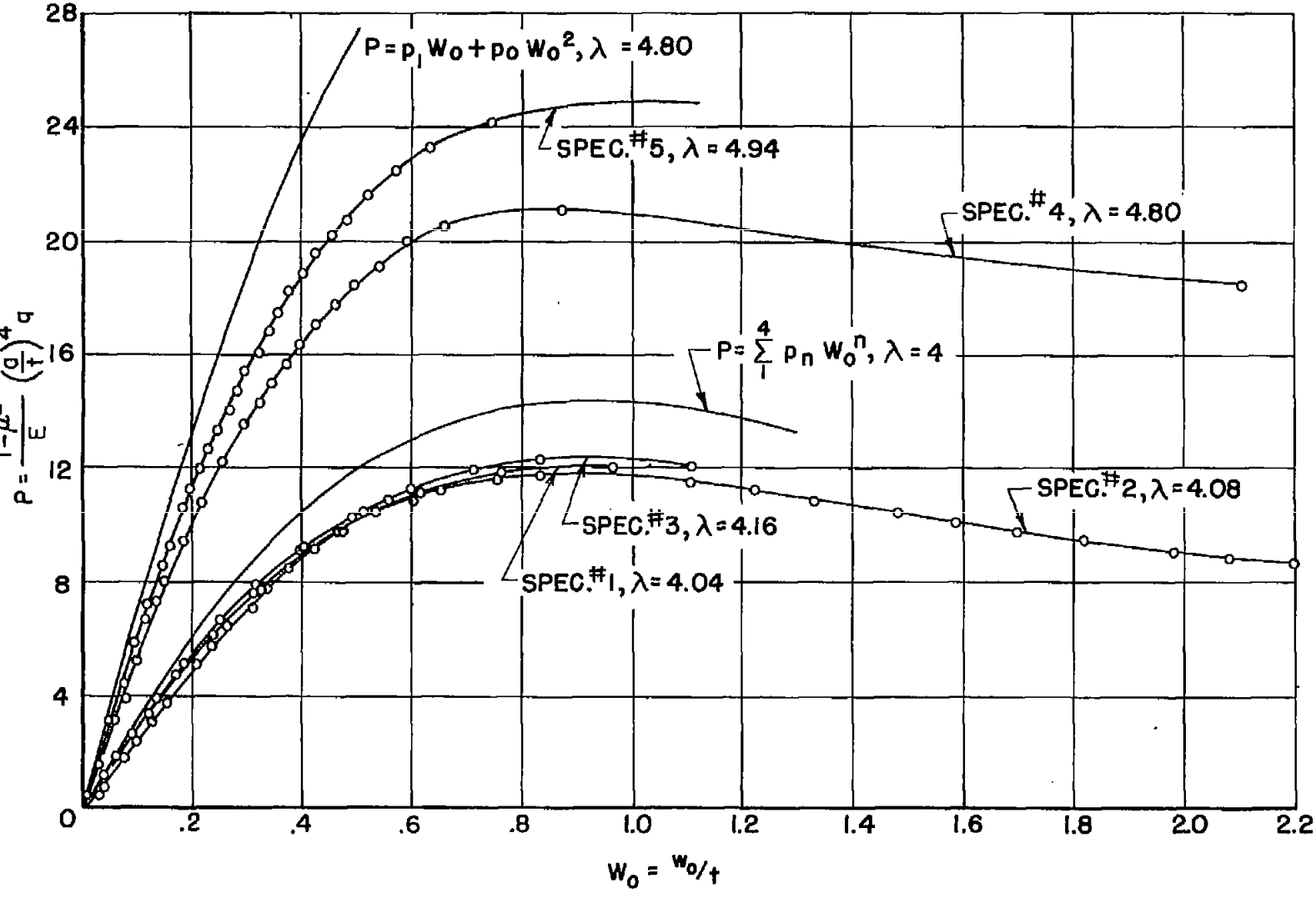

Figure 11.- Comparison of experimental pressure - center-deflection curves with theoretical results.

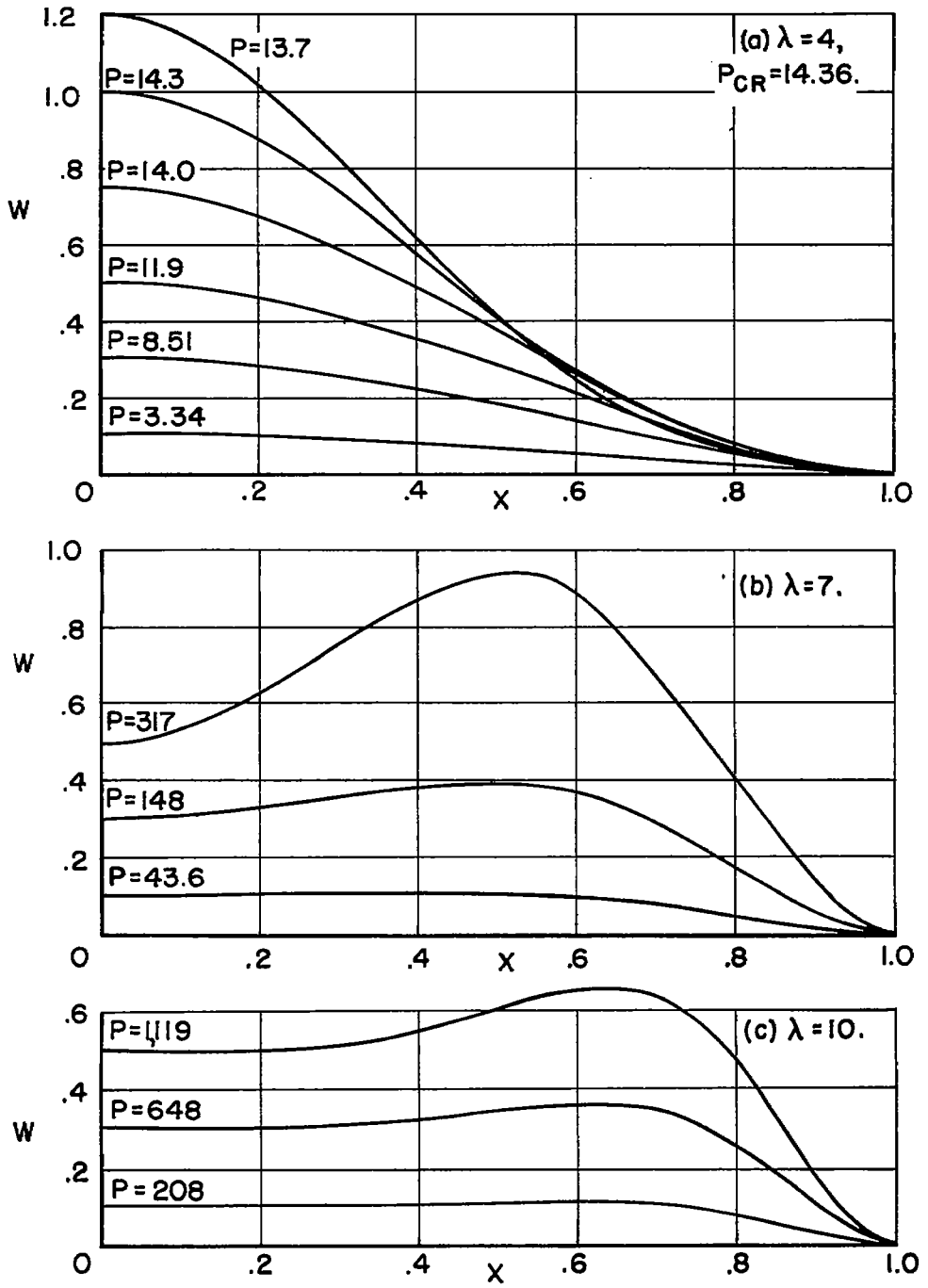

Figure 12.- Deflection modes for $\lambda = 4$, 7, and 10. For $\lambda = 4$ and 7, $W = \sum_{n=1}^{4} w_n W_o^n$; for $\lambda = 10$, $W = \sum_{n=1}^{2} w_n W_o^n$.

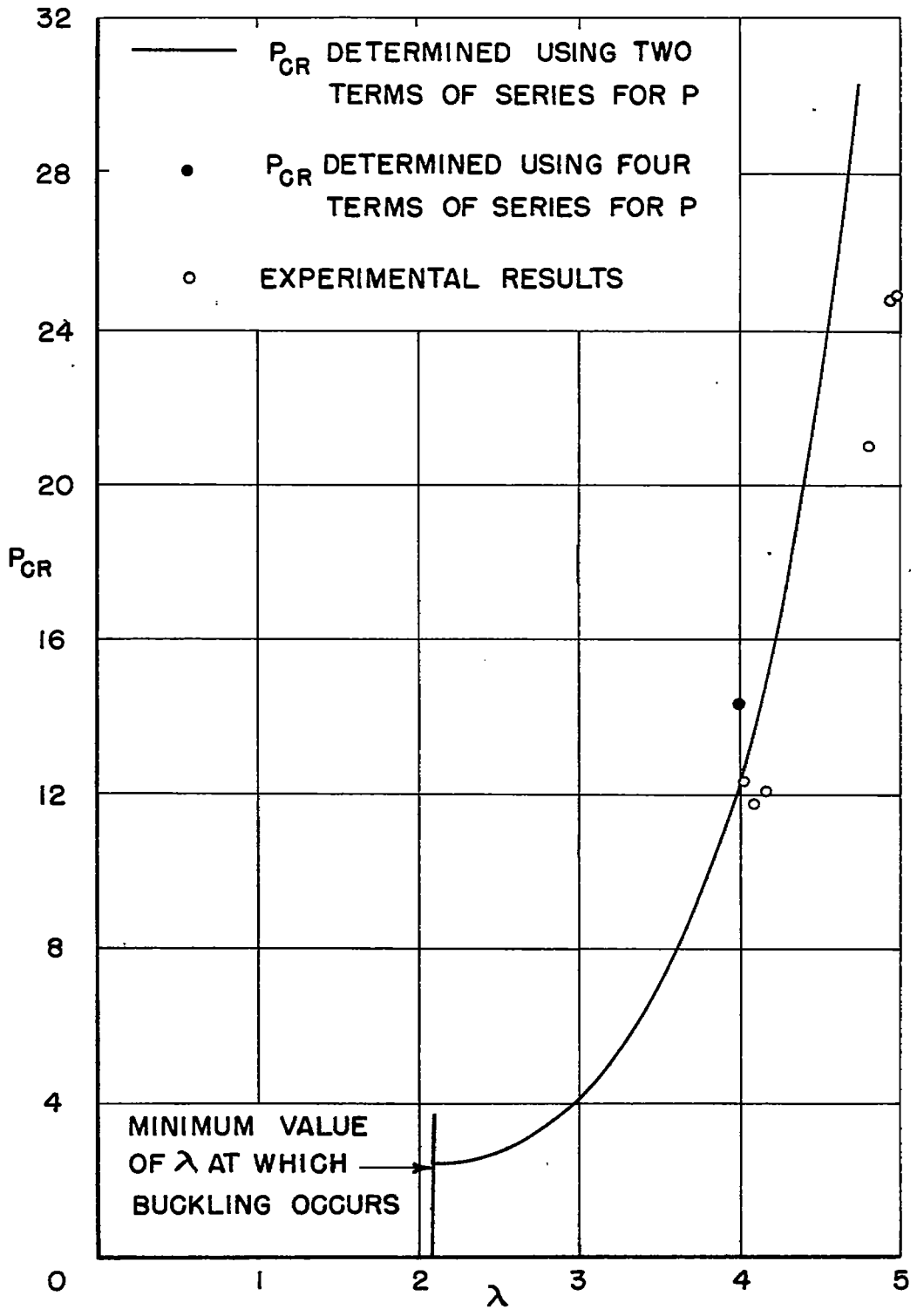

Figure 13.- Comparison of experimental buckling loads with theoretical values.

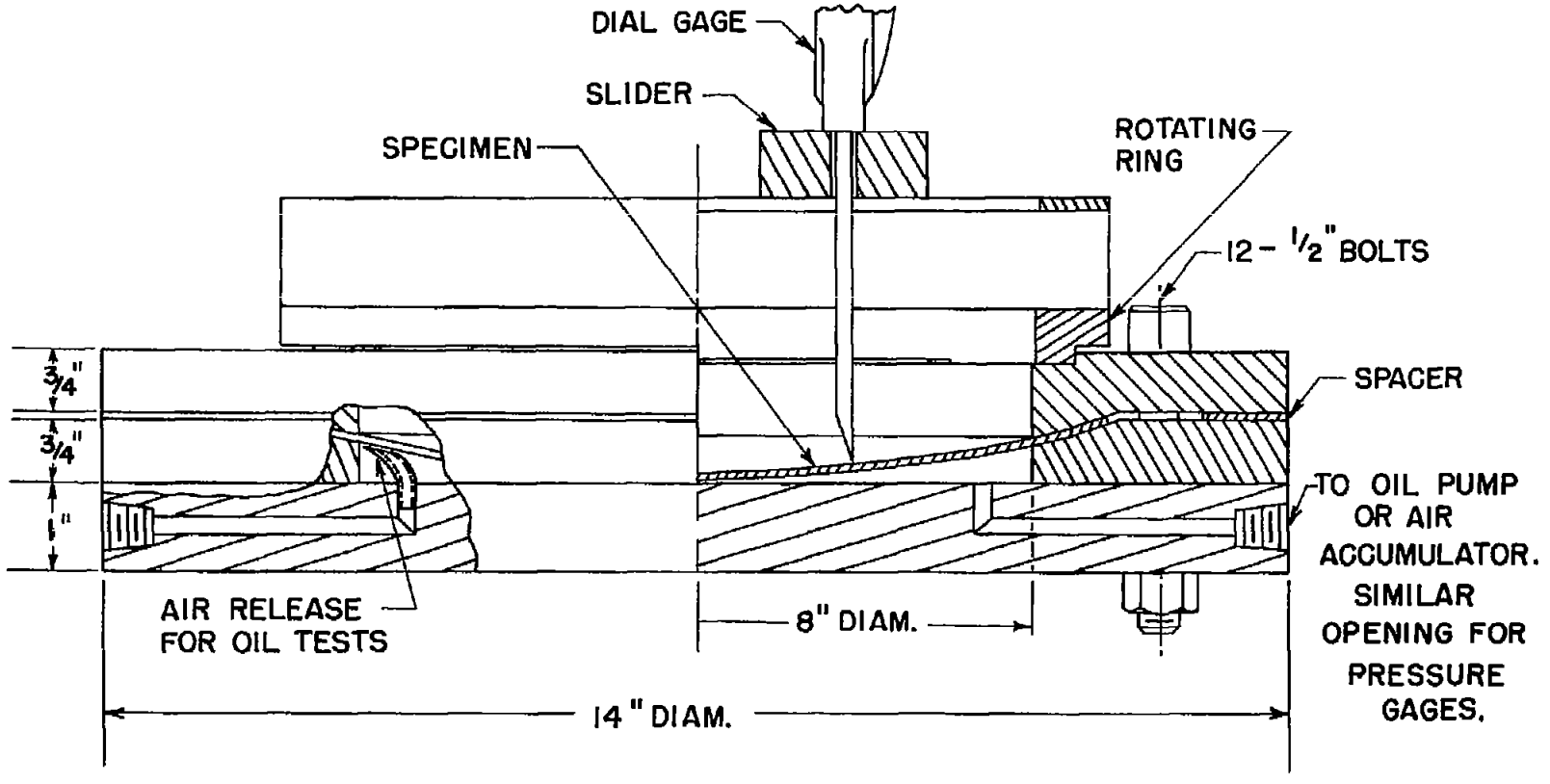

Figure 14.- Testing jig.

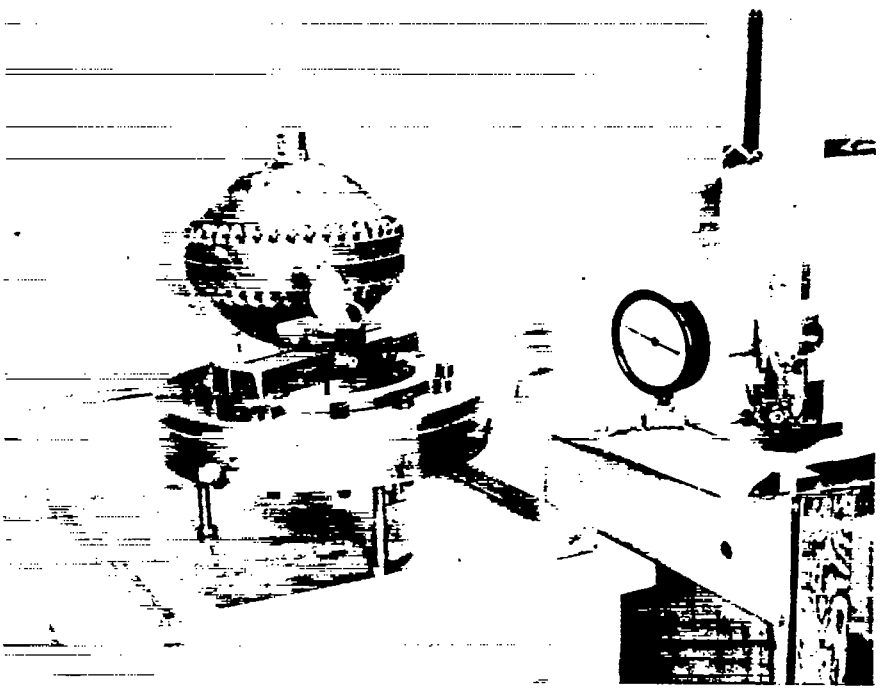

Figure 15.- View of testing fixture. L-84888

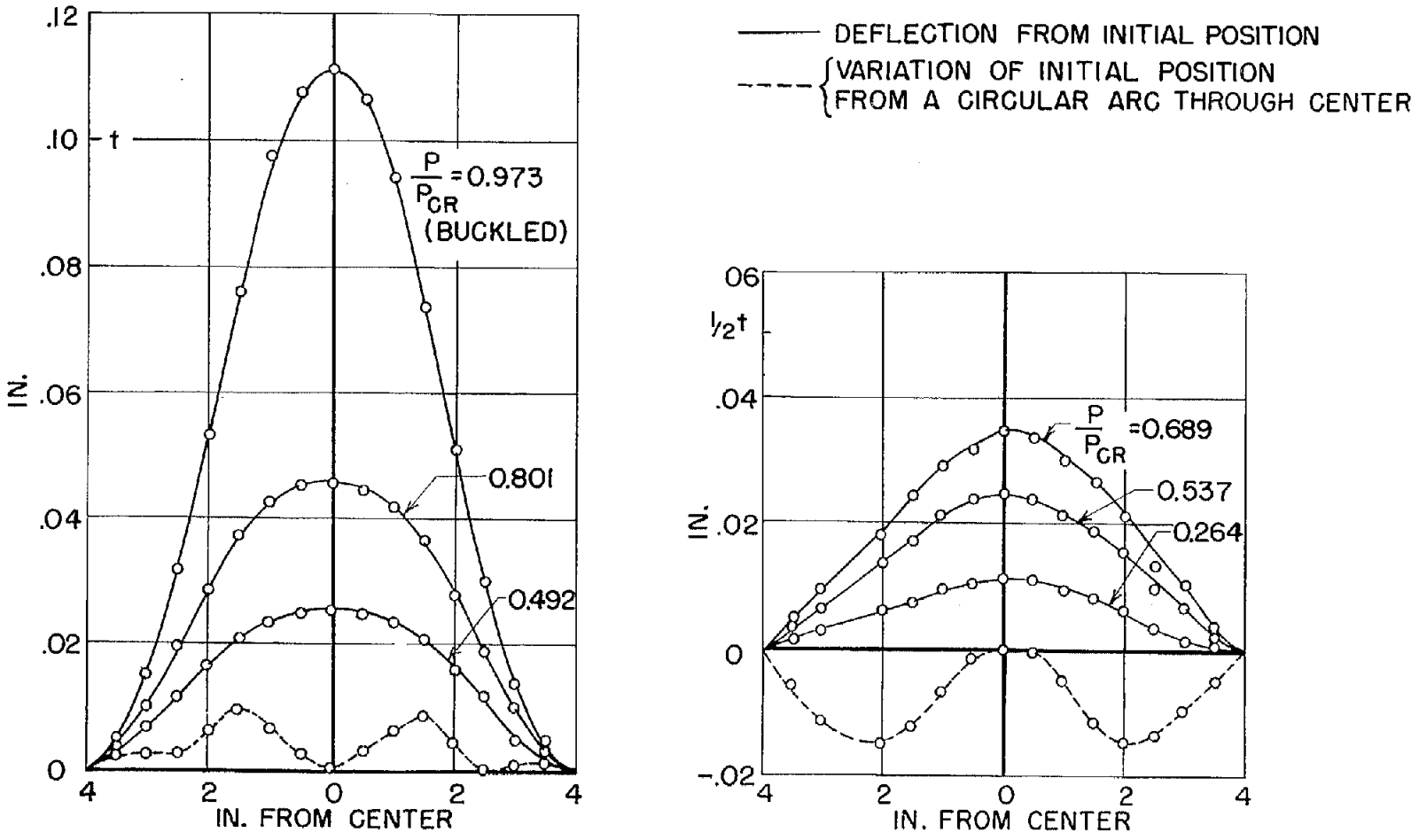

(a) Specimen 1; $\lambda = 4.04$;
$h = 0.251$ inch; $P_{cr} = 12.3$;
oil loading.

(b) Specimen 5; $\lambda = 4.94$;
$h = 0.376$ inch; $P_{cr} = 24.8$;
oil loading.

Figure 16.- Experimental deflection shapes.

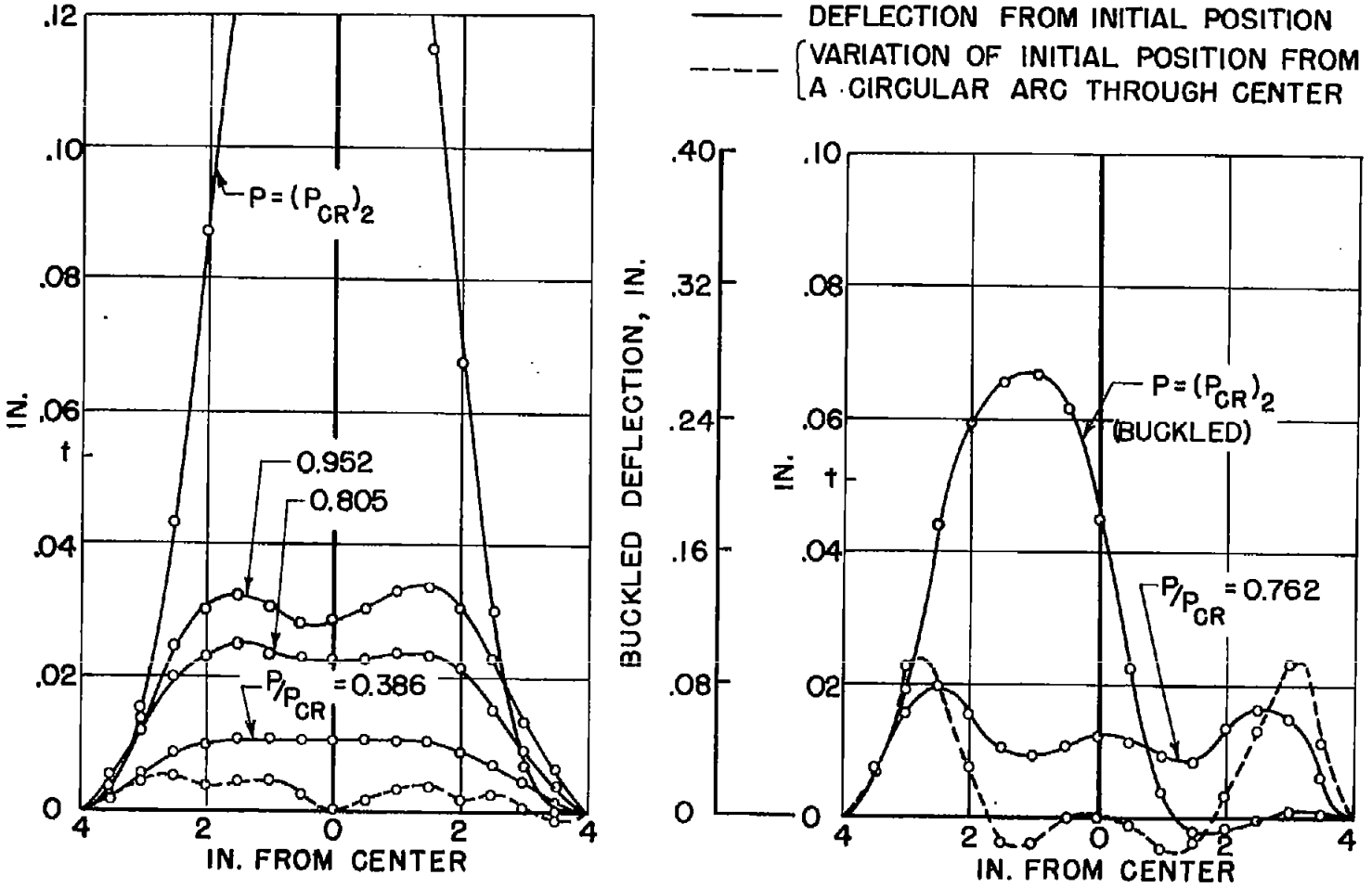

(c) Specimen 6; $\lambda = 5.45$;
$h = 0.240$ inch; $P_{cr} = 61.3$;
oil loading.

(d) Specimen 11; $\lambda = 7.40$;
$h = 0.422$ inch; $P_{cr} = 135.9$;
oil loading.

Figure 16.- Continued.

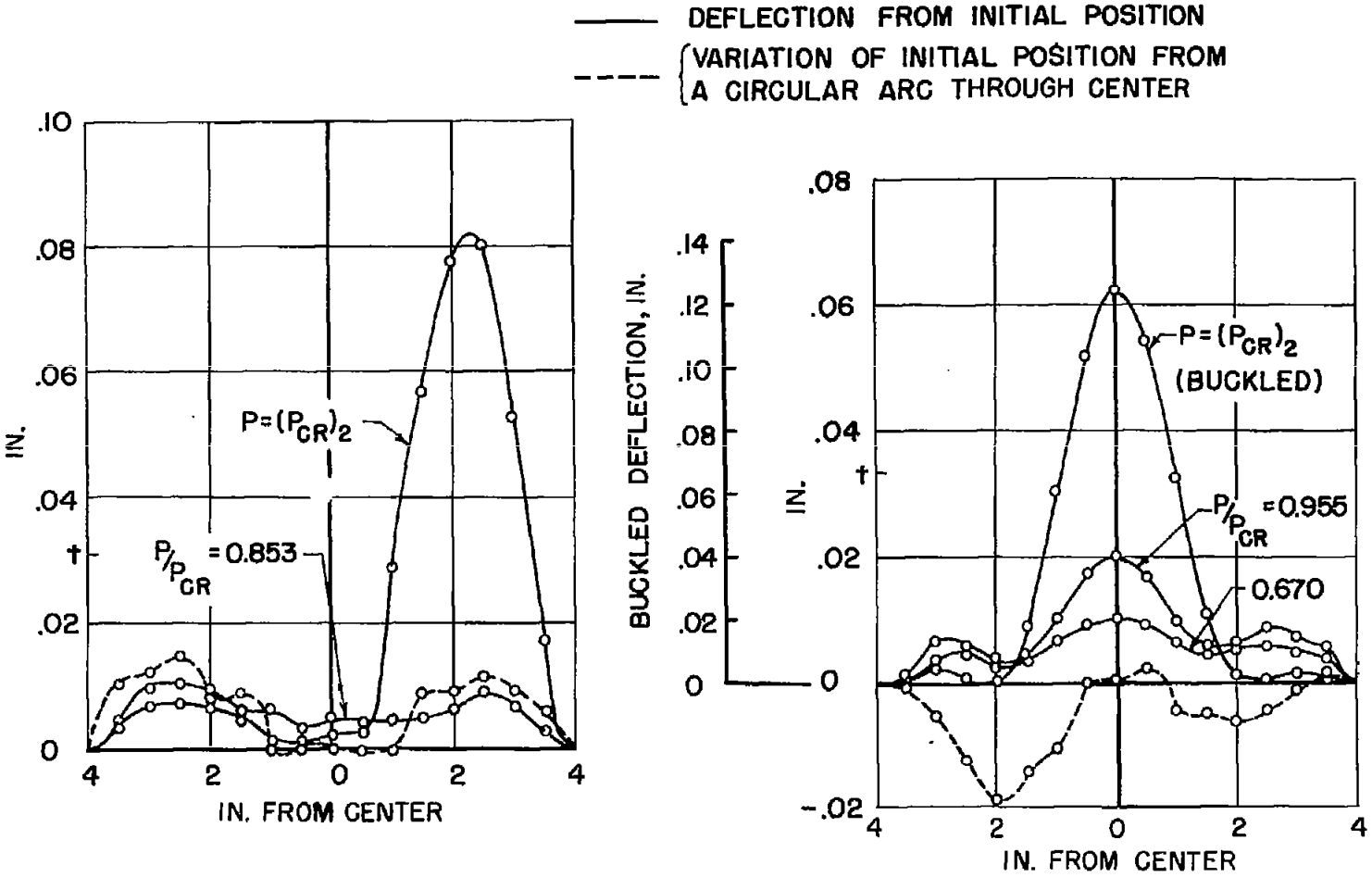

(e) Specimen 12; $\lambda = 8.59$;
$h = 0.361$ inch; $P_{cr} = 200.6$;
oil loading.

(f) Specimen 16; $\lambda = 8.98$;
$h = 0.410$ inch; $P_{cr} = 254.5$;
oil loading.

Figure 16.- Continued.

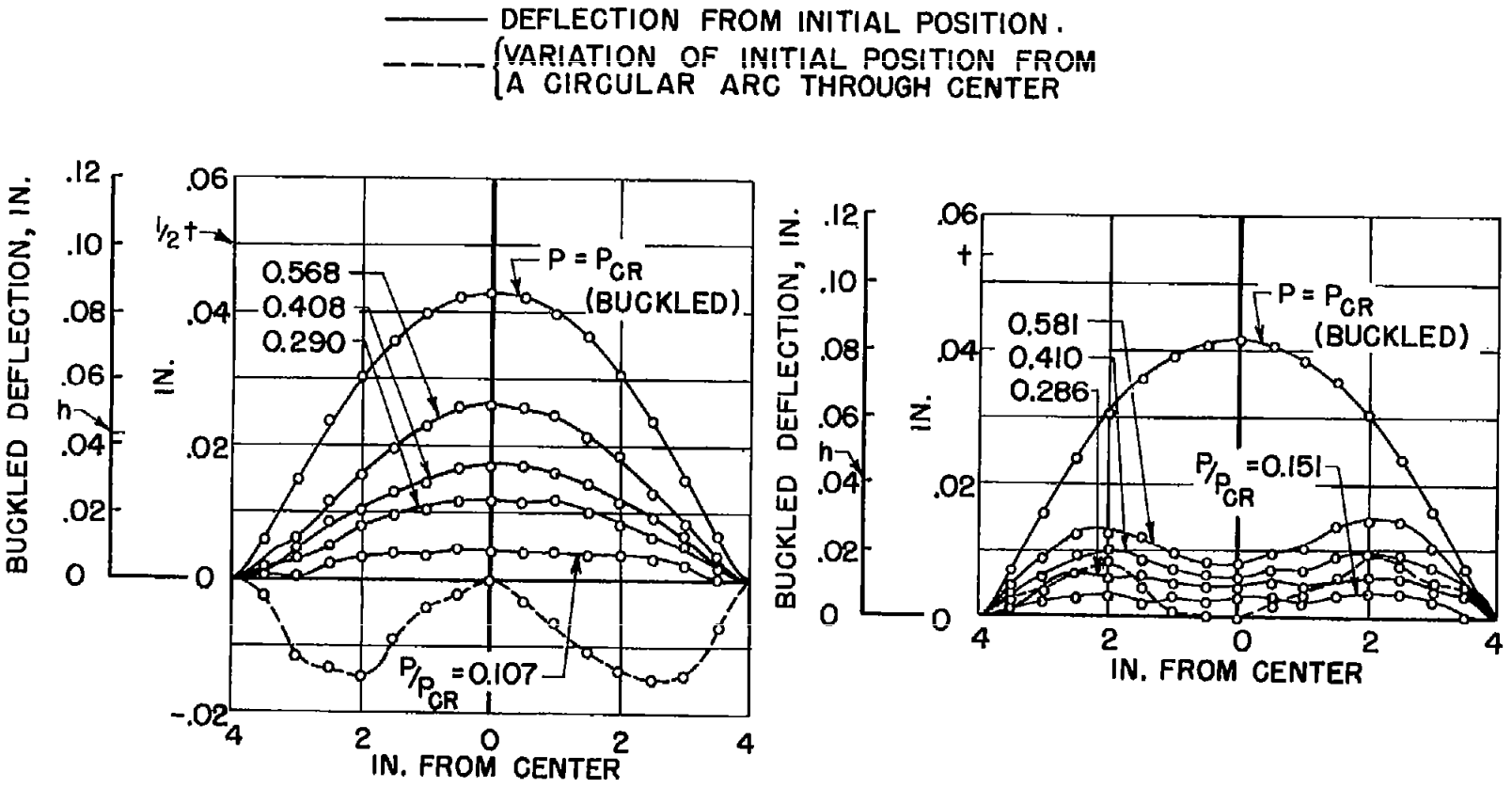

(g) Specimen 19; $\lambda = 5.26$;
$h = 0.426$ inch; $P_{cr} = 33.8$;
air pressure loading.

(h) Specimen 21; $\lambda = 7.10$;
$h = 0.413$ inch; $P_{cr} = 143$;
air pressure loading.

Figure 16.- Concluded.

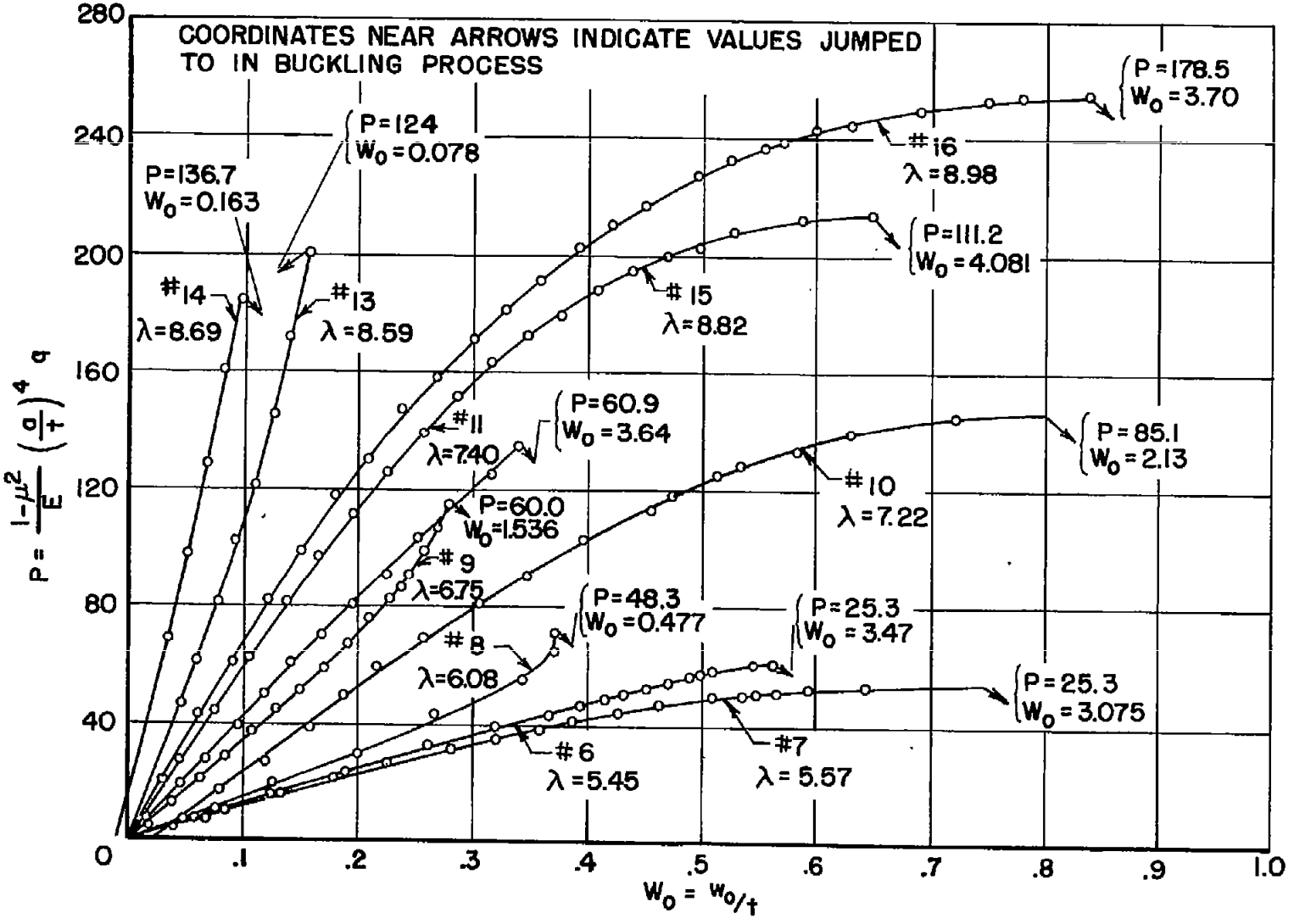

Figure 17.- Experimental pressure - center-deflection curves.

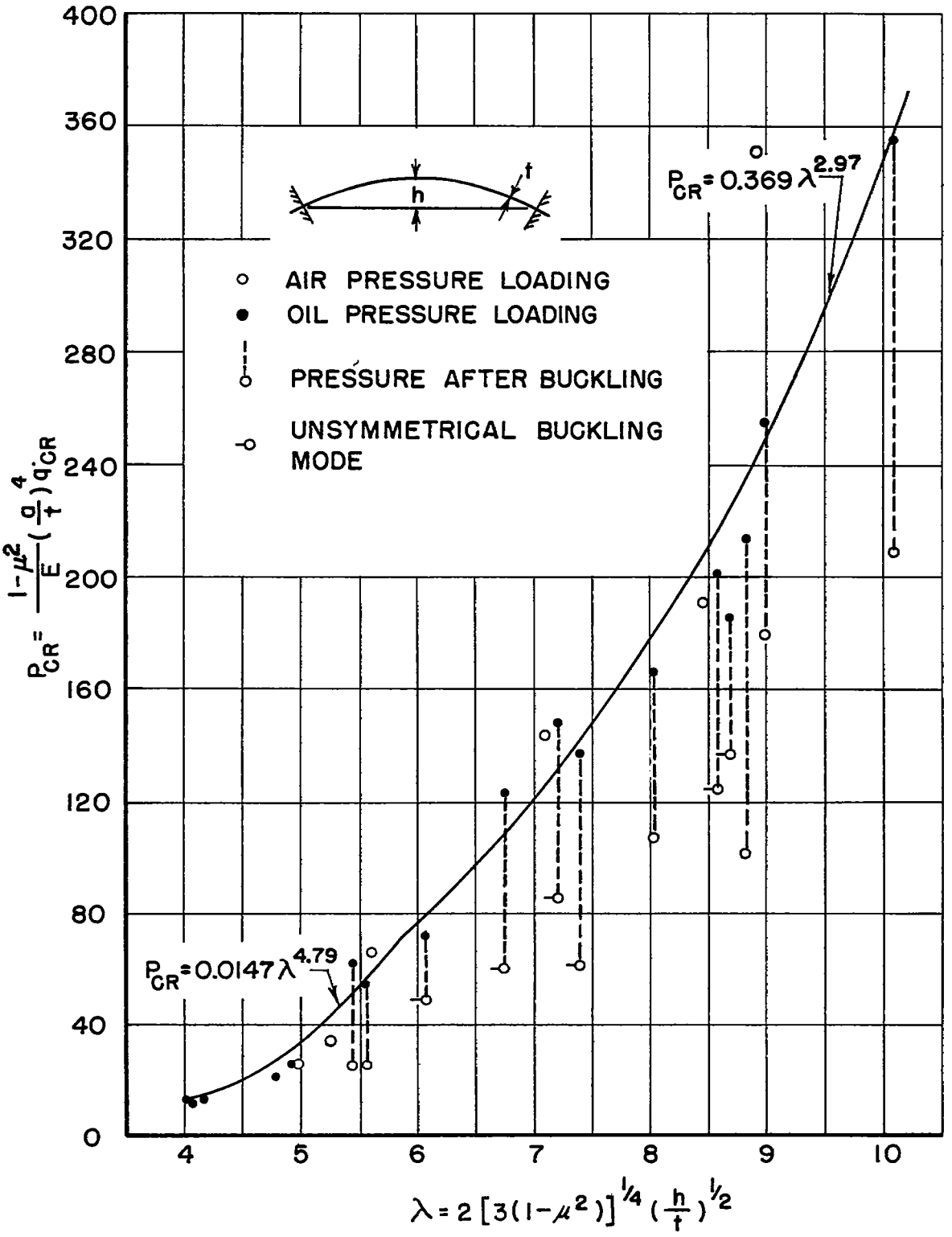

Figure 18.- Experimental results.

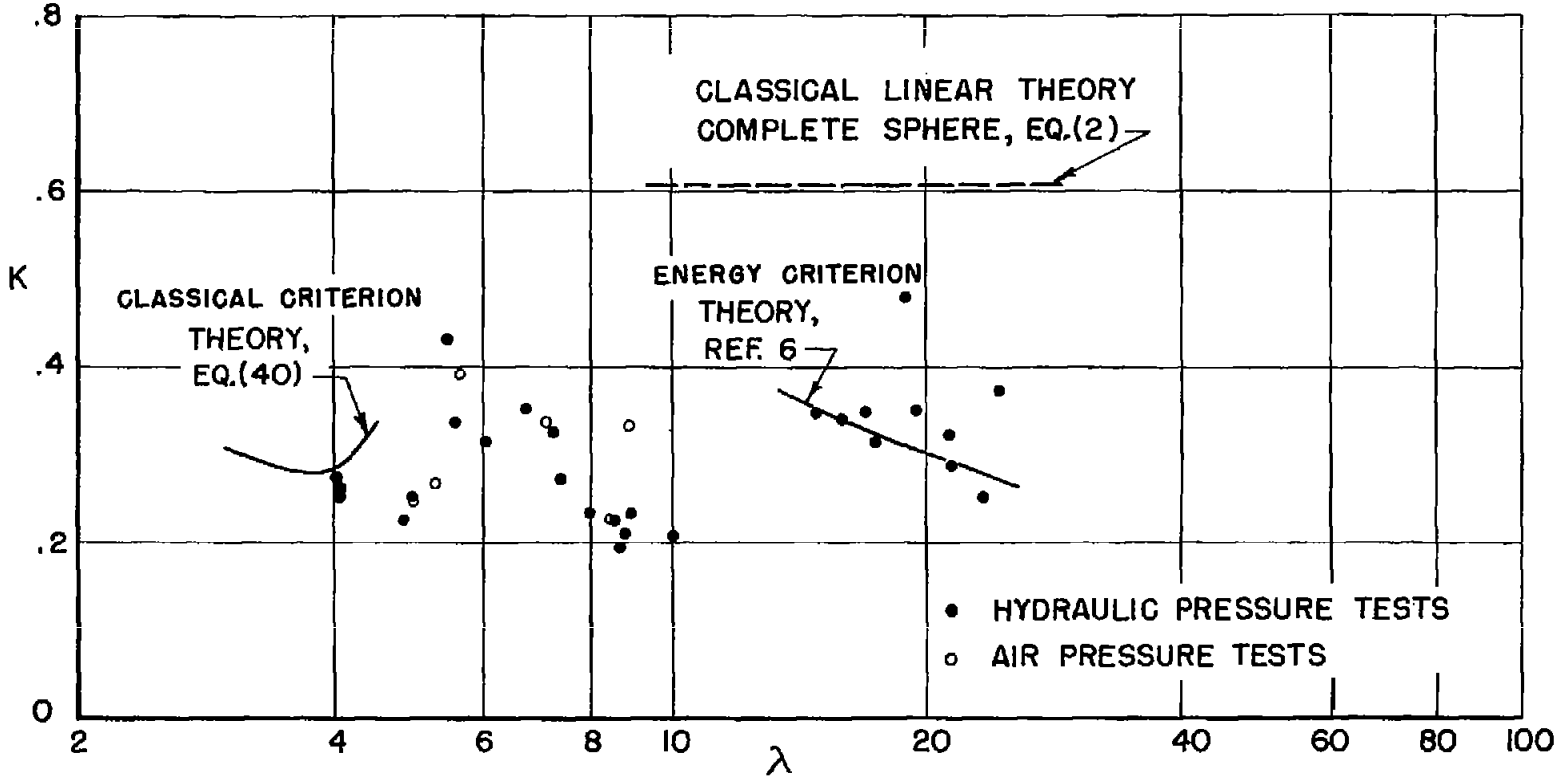

Figure 19.- Comparison of theory and experiment. $K = \frac{\sigma_{cr} R}{Et} = \frac{1}{2E}\left(\frac{R}{t}\right)^2 q_{cr}$;

$$\lambda = \left[12\left(1 - \mu^2\right)\right]^{1/4} \frac{a}{\sqrt{Rt}} \quad \text{or} \quad \left[12\left(1 - \mu^2\right)\right]^{1/4} \sqrt{\frac{R}{t}} \sin \beta.$$

NACA-Langley - 8-11-54 - 1000